iScience

CellPress
OPEN ACCESS

Article

BATTLE: Genetically Engineered Strategies for Split-Tunable Allocation of Multiple Transgenes in the Nervous System

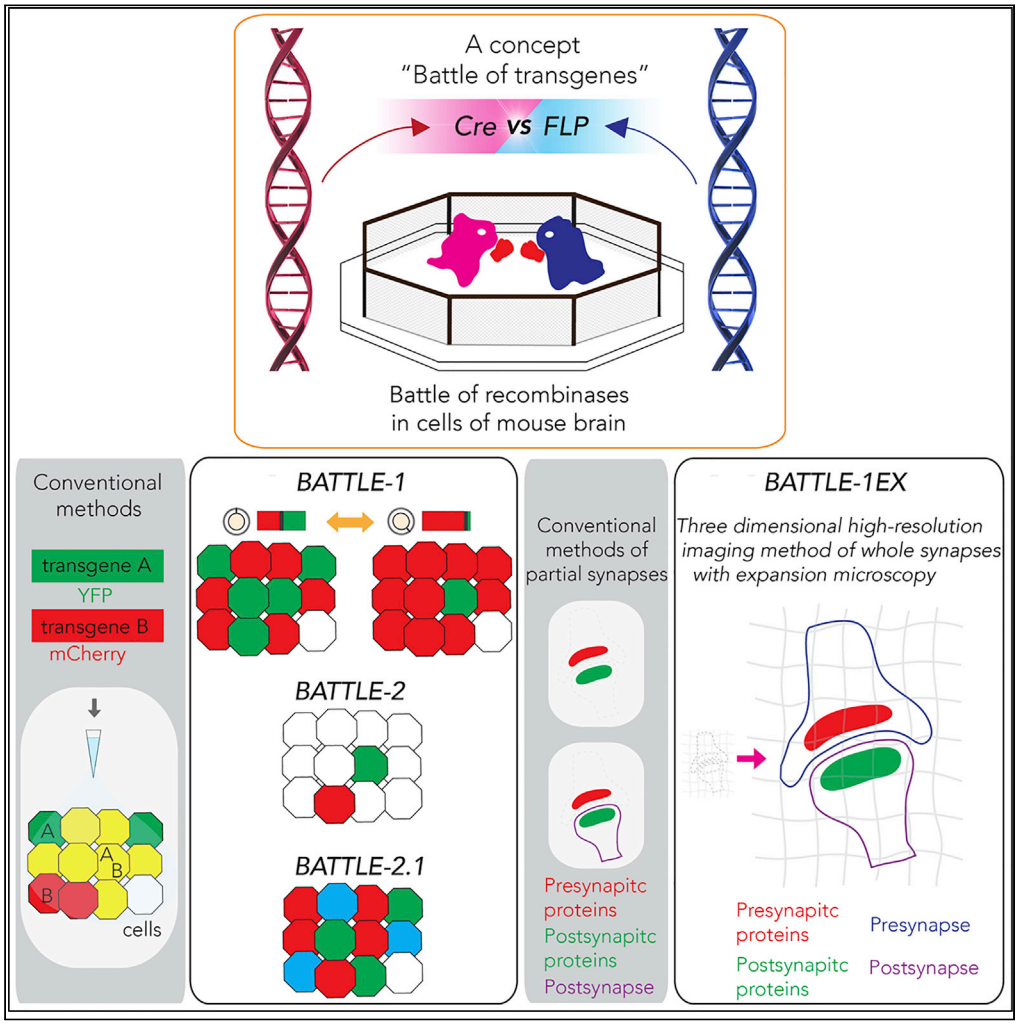

Keigo Kohara, Akitoshi Inoue, Yousuke Nakano, ..., Masato Maruyama, Ryosuke Baba, Chiho Kawashima

koharake@hirakata.kmu.ac.jp

HIGHLIGHTS

Generation of *BATTLE*-recombinase systems for allocation of multiple transgenes

Split-tunable allocation in *BATTLE*-1 and multi-sparse allocation in *BATTLE*-2

Clear and strong labeling of dendrites and axons using *BATTLE*-2

3D high-resolution imaging of whole synapses in hippocampus in *BATTLE*-1EX

Kohara et al., iScience *23*, 101248
June 26, 2020
https://doi.org/10.1016/j.isci.2020.101248

iScience

CellPress
OPEN ACCESS

Article

BATTLE: Genetically Engineered Strategies for Split-Tunable Allocation of Multiple Transgenes in the Nervous System

Keigo Kohara,[1,9,10,*] Akitoshi Inoue,[2,9] Yousuke Nakano,[3] Hirokazu Hirai,[4,5] Takuya Kobayashi,[2,6] Masato Maruyama,[3,7] Ryosuke Baba,[1] and Chiho Kawashima[1,8]

SUMMARY

Elucidating fine architectures and functions of cellular and synaptic connections requires development of new flexible methods. Here, we created a concept called the "battle of transgenes," based on which we generated strategies using genetically engineered battles of multiple recombinases. The strategies enabled split-tunable allocation of multiple transgenes. We demonstrated the versatility of these strategies and technologies in inducing strong and multi-sparse allocations of multiple transgenes. Furthermore, the combination of our transgenic strategy and expansion microscopy enabled three-dimensional high-resolution imaging of whole synaptic structures in the hippocampus with simultaneous visualizations of endogenous synaptic proteins. These strategies and technologies based on the battle of genes may accelerate the analysis of whole synaptic and cellular connections in diverse life science fields.

INTRODUCTION

Genes work cooperatively, competitively, and sometimes selfishly in the cells of the body (Dawkins, 1976). Cellular and synaptic connections are essential for almost all mammalian functions (Gumbiner, 1996; Südhof and Malenka, 2008). Genetic labeling of small groups of cells and synaptic structures is crucial to understanding the basal and functional mechanisms of the brain and body (Arenkiel and Ehlers, 2009). Blended expressions of multicolored fluorescent proteins are widely used for labeling neurons in neuroscience studies (Livet et al., 2007; Weissman and Pan, 2015; Sakaguchi et al., 2018), despite limitations in flexibility and tunability. To date, considerable efforts have been made to visualize and dissect whole synaptic structures using light microscopy (Nimchinsky et al., 2002; Rochefort and Konnerth, 2012), but most of these studies only succeeded in labeling half of the synaptic structures (Nimchinsky et al., 2002; Rochefort and Konnerth, 2012; Chen et al., 2015; Tillberg et al., 2016; Asano et al., 2018) such as spines or presynaptic terminals alone.

In this study, we created a concept called the "battle of the transgenes." Based on this concept, we designed three strategies, named *BATTLE*-1, 2, and 2.1 enabling splittable, tunable, intense, multi-sparse, triple splittable allocation of transgenes. *BATTLE*-1 used two genetically engineered recombinase proteins and induced recombinase fights for the mutually exclusive allocation of transgenes. *BATTLE*-2 used two genetically engineered recombinase proteins and a genetically engineered shadow recombinase protein to induce intense, tunable, and multiple sparse allocation of transgenes. *BATTLE*-2.1 used three genetically engineered recombinase proteins to induce triple splittable allocation of transgenes.

We combined *BATTLE*-1 with a method called *expansion microscopy* (ExM) (Chen et al., 2015; Tillberg et al., 2016; Asano et al., 2018), a high-resolution method that allows three-dimensional (3D) high-resolution imaging of whole, synaptic structures of hippocampal neural circuits. We called this *BATTLE*-1EX.

RESULTS

Battle of Recombinases and Genetically Engineered Strategies, *BATTLE*-1

To establish the concept of the battle of transgenes, we generated genetically battle-oriented recombinase proteins. Cyclization recombination (Cre) and flippase O (FLPO) recombinase proteins can originally excise a transgene flanked by two similar recombinase recognition sites (Nagy, 2000) (such as *loxP* and

[1]Department of Cellular and Functional Biology, Institute of Biomedical Science, Kansai Medical University, Hirakata, Osaka 573-1010, Japan

[2]Department of Medical Chemistry, Kansai Medical University, Graduate School of Medicine, Hirakata, Osaka 573-1010, Japan

[3]Department of Anatomy, Kansai Medical University, Graduate School of Medicine, Hirakata, Osaka 573-1010, Japan

[4]Department of Neurophysiology and Neural Repair, Gunma University Graduate School of Medicine, Maebashi, Gunma 371-8511, Japan

[5]Research Program for Neural Signalling, Division of Endocrinology, Metabolism and Signal Research, Gunma University Initiative for Advanced Research, Maebashi, Gunma 371-8512, Japan

[6]Japan Agency for Medical Research and Development (AMED), Core Research for Evolutional Science and Technology (CREST), 2-5-1 Shinmachi, Hirakata, Osaka 573-1010, Japan

[7]Faculty of Pharmaceutical Sciences, Graduate School of Medicine, Dentistry and Pharmaceutical Sciences, Okayama University, Okayama 700-8530, Japan

[8]Department of Bioscience, Osaka College of High Technology, Osaka 532-003, Japan

[9]These authors contributed equally

[10]Lead Contact

*Correspondence: koharake@hirakata.kmu.ac.jp

https://doi.org/10.1016/j.isci.2020.101248

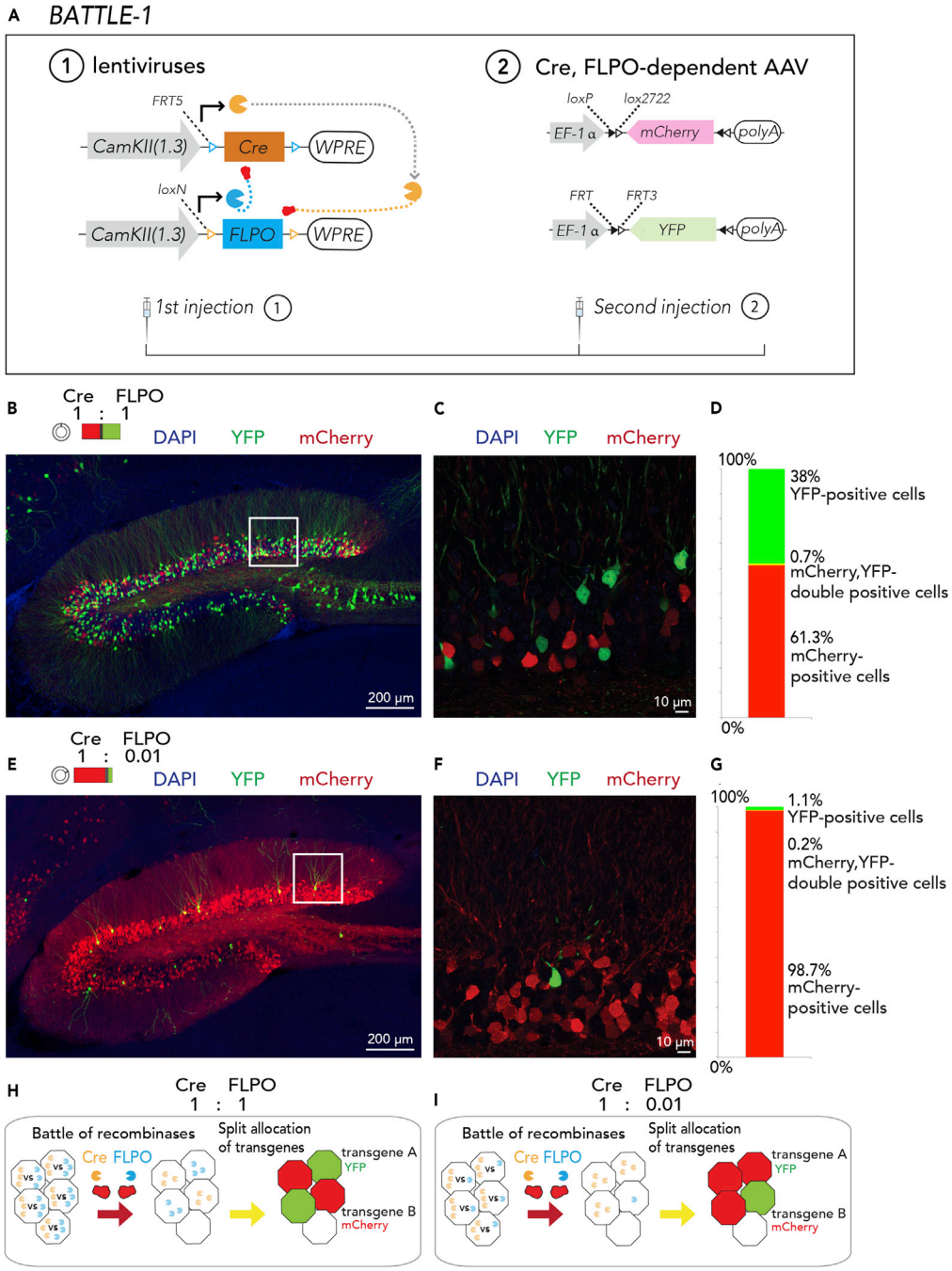

Figure 1. Battle of Recombinases

BATTLE-1: split-tunable allocation of transgenes by recombinase "fights."

(A) In the *BATTLE*-1 technology, Cre and FLPO are expressed under the control of CamKIIa promoter. The Cre transgene flanked by two FRT5 is designed to be a target of the FLPO recombinase. The FLPO transgene flanked by two loxN is designed to be a target of the Cre recombinase. Cre- and FLPO-dependent AAVs expressing mCherry and YFP, respectively, were used.

(B) Representative maximum intensity projection image of injected hippocampus. When the Cre to FLPO ratio was 1:1, the splitting allocation of YFP and mCherry was observed in hippocampal neurons.

(C) Magnified confocal image of the boxed area in (B).

(D) Quantification of percentage of cells expressing fluorescent proteins in the dentate gyrus.

Figure 1. *Continued*

(E) Representative maximum intensity projection image of injected hippocampus. When the ratio of Cre to FLPO was 1:0.01, most of the cells expressed mCherry, whereas few cells expressed YFP in the hippocampus.

(F) Magnified confocal image of the boxed area in (E).

(G) Quantification of percentage of cells expressing fluorescent proteins in the dentate gyrus.

(H) Illustration shows the battle of recombinases and *BATTLE*-1 system at a Cre to FLPO ratio of 1:1. After the first injection of mixed viruses, Cre and FLPO started recombinase battles in each infected neuron. Then, only the winning recombinase survived to induce its specific mutually exclusive allocation of transgenes (mCherry or YFP).

(I) Illustration shows the battle of recombinases and *BATTLE*-1 system at Cre to FLPO ratio of 1:0.01. In this situation, Cre wins over FLPO in many cells. Then mCherry is allocated in many cells, whereas YFP is allocated in a few cells.

flippase recognition target [FRT]). We designed multiple battle-oriented recombinases by aligning a Cre transgene flanked by two FRT mutant sites (Schlake and Bode, 1994) (FRT5) and an FLPO transgene flanked by two loci of X-over P1 (*loxP*) mutant sites (Livet et al., 2007) (loxN, Figure 1A). In this configuration, Cre is oriented to excise the FLPO transgene, which is then oriented to excise the Cre transgene.

To achieve the battle of transgenes in the mouse brain, we simultaneously injected lentiviruses encoding Cre flanked with FRT5 and ones encoding FLPO flanked with loxN at the same ratio (Cre:FLPO = 1:1) into the mouse hippocampus. Three weeks later, we injected Cre- and FLPO-dependent adeno-associated viruses (AAVs) expressing mCherry and yellow fluorescent protein (YFP), respectively, into the same region. YFP and mCherry were co-expressed with CamKIIa proteins in hippocampal neurons under the control of the CamKIIa (1.3 kb) promoter, indicating their specific expression in excitatory neurons (Benson et al., 1992) (CamKIIa+:100% of 148 mCherry-positive neurons, 100% of 101 YFP-positive neurons, and 100% of one mCherry-YFP double-positive neuron in the dentate gyrus, N = 3 mice, Figure S1).

Mixed viral infections mostly induce co-allocation of multiple transgenes in many cases (Weissman and Pan, 2015; Sakaguchi et al., 2018; Gomez-Nicola et al., 2014; Chan et al., 2017). We observed that YFP and mCherry were separately allocated in a majority of the fluorescence-positive neurons in the dentate gyrus (Figures 1B–1D, mCherry+:YFP+:mCherry-YFP double+ = 61.3% ± 5.8%:38% ± 5.8%:0.7% ± 0.2%, mean ± SEM; n = 827 granule neurons, N = 5 mice) and in the CA2-3 region of the hippocampus (mCherry+:YFP+:mCherry-YFP double+ = 78% ± 2.7%:21.4% ± 2.7%:0.6% ± 0.4%, mean ± SEM; n = 292 pyramidal neurons in CA2-3, N = 5 mice). Only a few neurons showed co-allocation of the transgenes (Figure 1D). Furthermore, we performed experiments with different dosages and observed similar splitting allocations of YFP and mCherry in dentate gyrus: 500 nL dosage, mCherry+:YFP+:mCherry-YFP double+ = 55.9% ± 1.5%:43.8% ± 1.6%:0.3% ± 0.1%, mean ± SEM, n = 1,111 granule neurons, N = 3 mice; 1,500 nL dosage, mCherry+:YFP+:mCherry-YFP double+ = 57.4% ± 1.4%:41.9% ± 1.6%:0.7% ± 0.3%, mean ± SEM, n = 1,458 granule neurons, N = 3 mice (Figure S2). These data suggest that the battle of multiple recombinases occurred and induced splitting allocation of YFP and mCherry. We called this strategy, based on the battle of multiple recombinases, *BATTLE*-1.

Then, we similarly injected *BATTLE*-1 lentiviruses at different ratios (Cre: FLPO = 1: 0.01, Figure 1E). Under this condition, we observed biased and splitting allocation of transgenes in the dentate gyrus (Figures 1E–1G, mCherry+:YFP+:mCherry-YFP double+ = 98.7% ± 0.2%:1.1% ± 0.2%:0.2% ± 0.1%, mean ± SEM, n = 1,153 granule neurons, N = 3 mice) and the CA2-3 region (mCherry+:YFP+:mCherry-YFP double+ = 96.2% ± 0.8%:3.6% ± 0.9%:0.1% ± 0.1%, mean ± SEM, n = 442 pyramidal neurons in the CA2-3 region, N = 4 mice). These data suggest that the dominant battle of recombinases induced biased allocation of transgenes in the hippocampus. Therefore, we generated the battle of transgenes in the mouse hippocampus (Figures 1H and 1I). For this purpose, we generated the *BATTLE*-1 technology enabling the splitting and tunable allocation of multiple transgenes in the mouse hippocampus.

BATTLE-2 for Splittable, Tunable, Intense, and Multi-sparse Allocation of Multiple Transgenes

Next, we created the *BATTLE*-2 technology based on genetically engineered "fights" between triple recombinases consisting of Cre transgene flanked by two FRT5-rox sites, FLPO transgene flanked by two loxN-rox sites, and Dre recombinase (Anastassiadis et al., 2009) transgene flanked by two FRT5-loxN sites (Figure 2A). We used Cre- and FLPO-dependent AAVs expressing mCherry and YFP, respectively, in *BATTLE*-2. Under this configuration, the Dre recombinase, referred to as "shadow fighter," did not induce the expression of specific transgenes. To test the *BATTLE*-2 technology, we simultaneously injected lentiviruses encoding Cre flanked with FRT5-rox, one encoding FLPO flanked with loxN-rox sites, and the one encoding a Dre transgene flanked by two FRT5-loxN sites at the same ratio (Cre:FLPO:Dre = 1:1:1, Figure 2A).

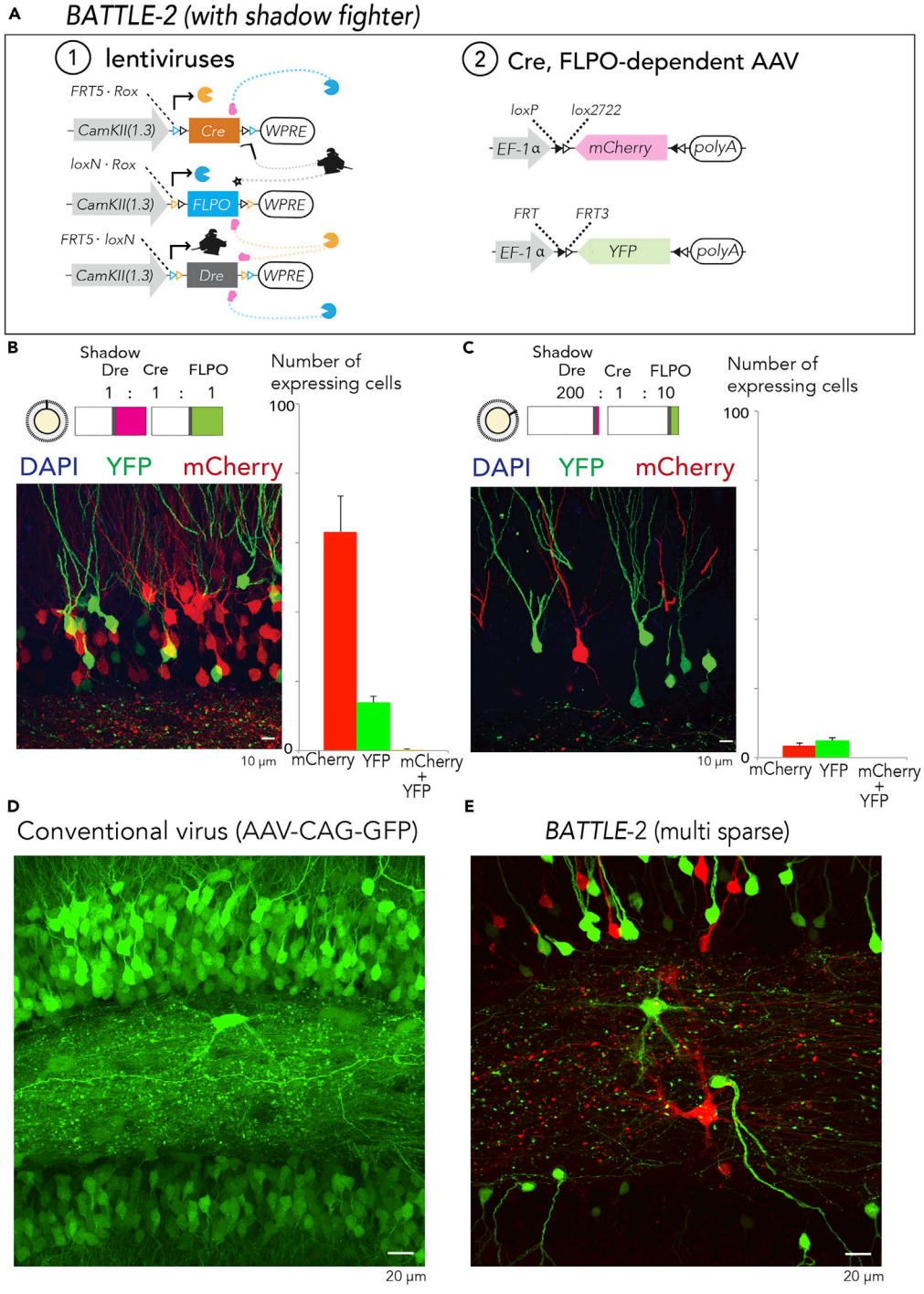

Figure 2. *BATTLE*-2 (with Shadow Fighter): Split-Tunable and Multi-sparse Allocation of Transgenes Using the Battle of the Recombinases

(A) In *BATTLE*-2 technology, Cre, FLPO, and Dre are expressed under the control of CamKIIa promoter. Then, Cre excises FLPO and Dre transgenes, whereas FLPO excises Cre and Dre transgenes. In addition, Dre excises FLPO and Cre transgenes. Using AAVs, Cre induces mCherry expression and FLPO induces YFP expression. However, Dre as a shadow fighter did not induce expression of transgenes.

(B) (Left) A representative maximum intensity projection image of dentate gyrus infected with *BATTLE*-2 system when the ratio of Dre:Cre:FLPO was 1:1:1. (Right) Quantification of cell number of neurons expressing fluorescent protein in the dentate gyrus. Data are represented as mean ± SEM.

Figure 2. *Continued*

(C) (Left) Representative maximum intensity projection image of dentate gyrus infected with *BATTLE*-2 system when the ratio of Dre:Cre:FLPO was 200:1:10. (Right) Quantification of cell number of neurons expressing fluorescent protein in the dentate gyrus. Data are represented as mean ± SEM.

(D) Representative maximum intensity projection image of dentate gyrus infected with conventional virus AAV-CAG-GFP. Note that the morphologies of mossy cells are unclear.

(E) Representative maximum intensity projection image of dentate gyrus infected with *BATTLE*-2 (double sparse). Note that the morphologies of multiple mossy cells are clear using *BATTLE*-2 double sparse expression.

Three weeks later, we injected Cre-dependent AAV expressing mCherry and FLPO-dependent one expressing YFP in the same region. YFP and mCherry were co-expressed with CamKIIa proteins in hippocampal neurons under the control of the CamKIIa (1.3 kb) promoter, indicating their specific expression in excitatory neurons (Figure S3). We observed splitting allocation of mCherry and YFP in the dentate gyrus (Figure 2B, mCherry+:63.1 ± 10.2, YFP+:13.9 ± 1.8, and mCherry-YFP double+:0.3 ± 0.2, mean ± SEM, number of expressing cells/400 μm^2, n = 618 granule neurons in the dentate gyrus, N = 3 mice) and CA2-3 (mCherry+:39.8 ± 8.5, YFP+:5.1 ± 1.4, and mCherry-YFP double+:0.6 ± 0.4, mean ± SEM, number of expressing cells/400 μm^2, n = 364 pyramidal neurons in CA2-3, N = 3 mice). Furthermore, we observed similar splitting allocation of mCherry and YFP in dentate gyrus with different dosages of mixed lentiviruses: 500 nL dosage, mCherry+:YFP+:mCherry-YFP double+ = 73.3% ± 4.1%:26.3% ± 4.1%:0.5% ± 0.3%, mean ± SEM, n = 569 granule neurons, N = 4 mice; 1,000 nL dosage, mCherry+:YFP+:mCherry-YFP double+ = 81.1% ± 1.7%:18.9% ± 1.7%:0.2% ± 0.2%, mean ± SEM, n = 618 granule neurons, N = 3 mice; 1,500 nL dosage, mCherry+:YFP+:mCherry-YFP double+ = 80.8% ± 2.5%:18.5% ± 2.4%:0.7 ± 0.3%, mean ± SEM, n = 674 granule neurons, N = 3 mice (Figure S4).

To achieve multiple sparse allocation of transgenes, we injected a lentivirus encoding Cre flanked with FRT5-rox, one encoding FLPO flanked with loxP-rox sites, and another encoding Dre transgene flanked by two FRT5-loxP sites (Cre:FLPO:Dre = 1:10:200), following Cre- and FLPO-dependent AAV injection. *BATTLE*-2 induced intense and double sparse allocation of mCherry and YFP in granule neurons of the dentate gyrus (Figure 2C, mCherry+:3.4 ± 0.9, YFP+:4.9 ± 0.8, and mCherry-YFP double+: 0, mean ± SEM, number of expressing cells/400 μm^2, n = 66 granule neurons in dentate gyrus, N = 4 mice) and pyramidal neurons in the CA2-3 (mCherry+:1.1 ± 0.4, YFP+:1.9 ± 0.3, and mCherry-YFP double+:0, mean ± SEM, number of expressing cells/400 μm^2, n = 14 pyramidal neurons in CA2-3, N = 6 mice).

In contrast to the excessively dense green protein fluorescence (GFP) expression with unclear cell morphologies induced by conventional viruses (Figure 2D), dendritic and axonal morphologies were strongly, sparsely, and clearly labeled using the *BATTLE*-2 technology (Figure 2E and Video S1).

Furthermore, we created Dre-dependent AAV expressing mTFP (Chuang et al., 2015; Ai et al., 2006). To confirm Dre-specific recombination of Dre-dependent AAV, crosstalk activities between Cre, FLPO, and Dre were examined. We did not observe crosstalk activities in our experimental conditions (Figure S5).

Using *BATTLE*-2 with this AAV, we observed triple splitting allocations of mTFP, YFP, and mCherry in granule neurons of the dentate gyrus and pyramidal neurons in the CA2-3 and called this *BATTLE*-2.1: 500 nL dosage, mCherry+:mTFP+: YFP+:mTFP-YFP double+:mTFP-mCherry double+:mCherry-YFP double+:triple+ = 62.3% ± 2.4%:18.5% ± 1.8%:18.5% ± 1.7%:0%:0.4% ± 0.2%:0.2% ± 0.2%:0%, mean ± SEM, n = 740 granule neurons, N = 4 mice; 1,000 nL dosage, mCherry+:mTFP+: YFP+:mTFP-YFP double+:mTFP-mCherry double+:mCherry-YFP double+:triple+ = 73.4% ± 2.8%:13.7% ± 1.5%:12.4% ± 1.8%:0%:0.4% ± 0.2%:0.3% ± 0.2%:0%, mean ± SEM, n = 910 granule neurons, N = 4 mice; 1,500 nL dosage, mCherry+:mTFP+: YFP+:mTFP-YFP double+:mTFP-mCherry double+:mCherry-YFP double+:triple+ = 71.6% ± 3%:11.7% ± 1.8%:16.2% ± 1.9%:0%:0.1% ± 0.1%:0.4% ± 0.2%:0%, mean ± SEM, n = 1,127 granule neurons, N = 4 mice (Figure 3, Figure S6).

High-Resolution Imaging of Whole Synaptic Structures Using Multicolor Immunohistochemistry with *BATTLE*-1EX

Conventional methods using AAV-expressing GFP did not clearly reveal whole synaptic structures (Figure 4A). To visualize whole structures of synaptic connections clearly, we combined *BATTLE*-1 with ExM (*BATTLE*-1EX), which is a high-resolution method (Figure 4B, top). Hippocampal slices infected by *BATTLE*-1 were expanded linearly by 4.1 times (Figure 4B bottom, Figure S7, 4.1 ± 0.0, mean ± SEM, n = 5

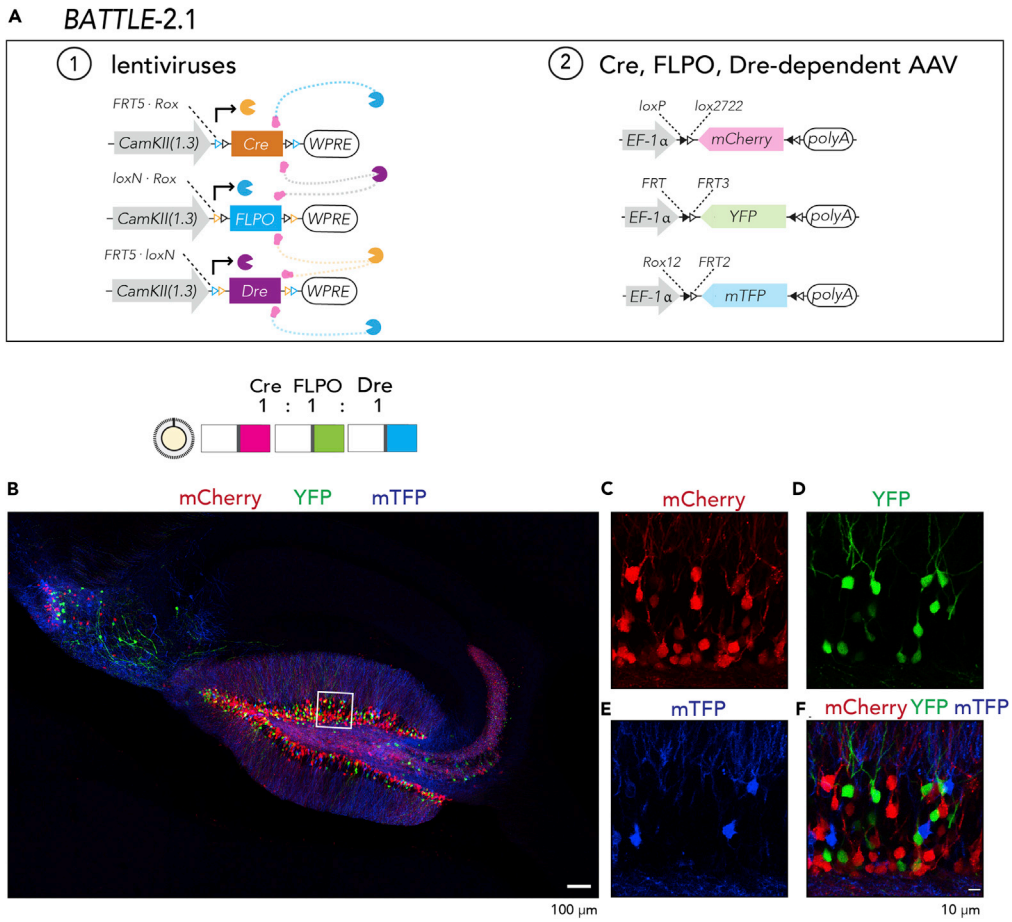

Figure 3. *BATTLE*-2.1: Triple Splitting Allocation of Transgenes Using the Battle of the Recombinases

(A) In *BATTLE*-2.1 technology, Cre, FLPO, and Dre are expressed under the control of CamKIIa promoter. Cre excises FLPO and Dre transgenes, whereas FLPO excises Cre and Dre transgenes. Dre excises FLPO and Cre transgenes. Using AAVs, Cre induces mCherry expression and FLPO induces YFP expression. In addition, Dre induces mTFP expression.

(B) A representative maximum intensity projection image of hippocampus infected with the *BATTLE*-2.1 system when the ratio of Dre:Cre:FLPO was 1:1:1. Scale bar, 100 um.

(C) Magnified maximum intensity projection image (6 μm thickness) of the boxed area in (B). Red color shows mCherry expression.

(D) Magnified maximum intensity projection image of the boxed area in (B). Yellow color shows YFP expression.

(E) Magnified maximum intensity projection image of the boxed area in (B). Blue color shows mTFP expression.

(F) Superposed maximum intensity projection image of the boxed area in (B). Red, yellow, and blue show mCherry, YFP and mTFP, respectively. Scale bar, 10 μm.

slices). Therefore, a lens with a diffraction limit of ~280 nm (60X, 1.2 numerical aperture water objective from Olympus) would attain an effective resolution of ~280 nm/4.1 ≈ 70 nm. In this area (44.3 μm × 44.3 μm × 6.8 μm), we observed that 14 YFP-positive presynaptic terminals stochastically formed the whole synapse with mCherry-positive postsynaptic spines of CA3 neurons. Other cases consisting of mCherry-positive presynaptic terminals with YFP-positive postsynaptic spines were also observed (see Figure 5B).

Using *BATTLE*-1EX, whole synaptic structures consisting of YFP-positive presynaptic terminals from the dentate gyrus and mCherry-positive postsynaptic spines of CA3 pyramidal neurons were clearly visualized (Figures 4C and S8). Furthermore, the localizations of Bassoon and Homer, which are presynaptic and post-synaptic proteins, respectively, were also simultaneously identified in whole synaptic structures (Figure 4C and 4D). We performed volume rendering, offering 3D whole synaptic structures and 3D localization of Bassoon and Homer of DG-CA3 synapses in the hippocampus (Figures 4E and 4F, Video S2). High-resolution imaging of the whole synaptic structures was performed at sequential z stacks (Figure 4G). We further

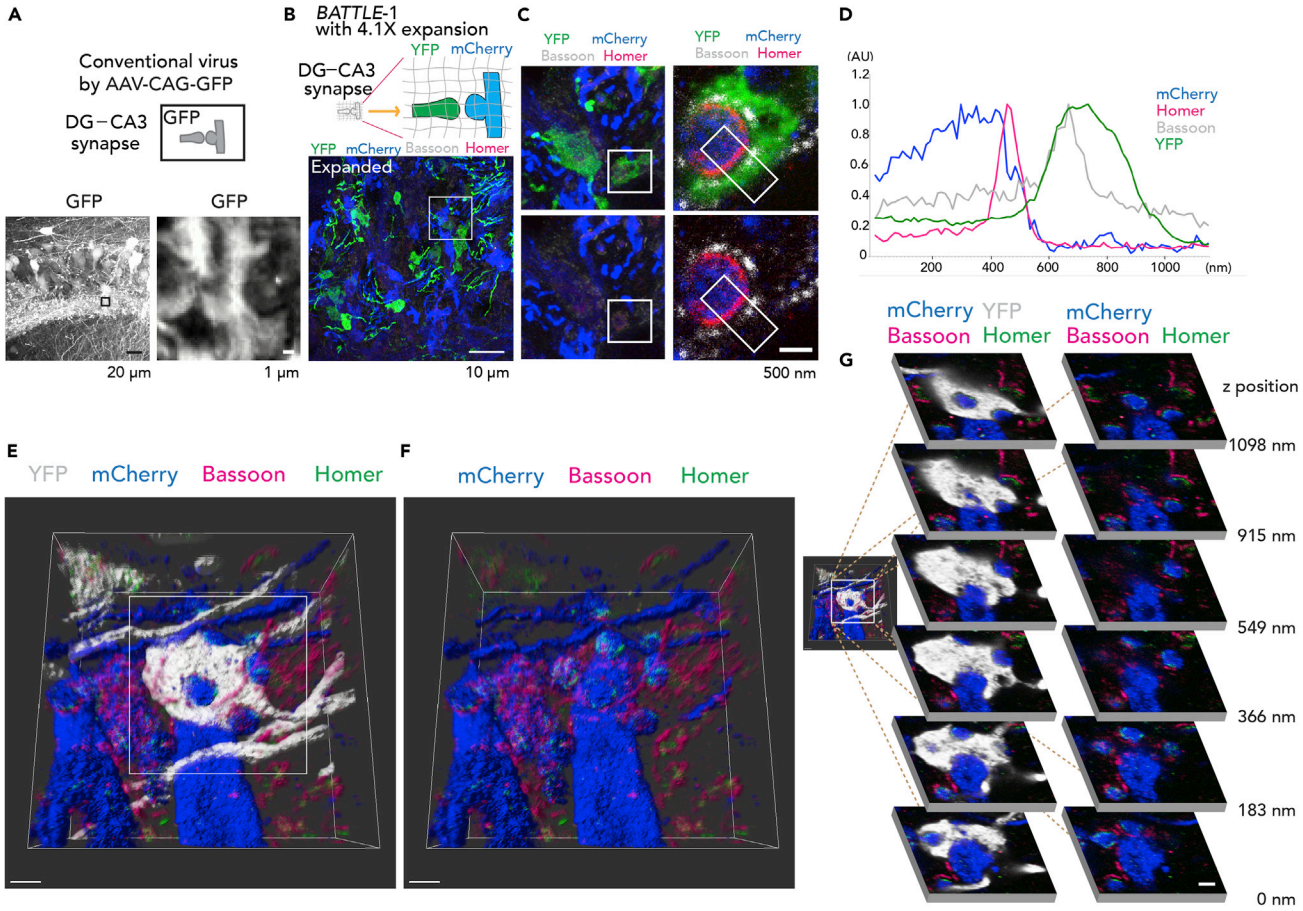

Figure 4. *BATTLE*-1EX: Three-Dimensional (3D) High-Resolution Imaging of Whole Synaptic Structures

(A) (Top) Illustration of DG-CA3 synapse visualized using AAV-CAG-GFP. (Left) Representative maximum intensity projection image in the CA3 region infected with conventional virus AAV-CAG-GFP. (Right) Magnified confocal image of boxed area to the left. Note unclear morphologies of whole synaptic structures of DG-CA3 synapses.

(B) (Top) Illustration showing *BATTLE*-1EX. *BATTLE*-1-infected slices are expanded using 4.1× expansion microscopy (ExM). (Bottom) Representative maximum intensity projection image of CA3 stratum lucidum of *BATTLE*-1EX slices.

(C) (Top left) Magnified maximum intensity projection image of boxed area in (B). (Top, right) Magnified confocal images of boxed area in (C) top left.

(D) Cross-sectional line profiles of fluorescent intensities in boxed region in (C) right.

(E) Representative volume-rendering 3D image of the whole synaptic structure of DG-CA3 synapses. Scale bar, 732 nm.

(F) Same volume-rendering 3D image in (D) without YFP.

(G) (Left) Magnified images of (E). (Right) the sequential z stack images of the boxed area in (left). Scale bar, 500 nm.

performed volume rendering (Figures 5A–5E) to visualize the 3D high-resolution whole synaptic structures of synapses from granule neurons to hilar mossy cells.

DISCUSSION

The concept, battle of transgenes, offers a theoretical and experimental base for the progress of research in the various scientific fields including life science, biotechnology, bioengineering technology, and artificial intelligence technology. *BATTLE*-recombinase systems, generated on this concept, are transgenic strategies for wide-scale studies of cellular and synaptic interactions in the life sciences and have two key advantages. First, they allow genetically engineered recombinases to "fight," and only the winning recombinase survives in the infected cells to induce its specific transgene allocation. Unlike other systems (Zong et al., 2005; Saunders et al., 2012; Lao et al., 2012; Tasic et al., 2012; Pontes-Quero et al., 2017), the subsequent mutually exclusive transgene allocation is flexible and tunable by simply changing the ratio of mixed *BATTLE*-recombinase viruses without re-designing basic constructs of the viral vectors. The interleaved strategy is based on the competition between two recombinases and is useful for splitting

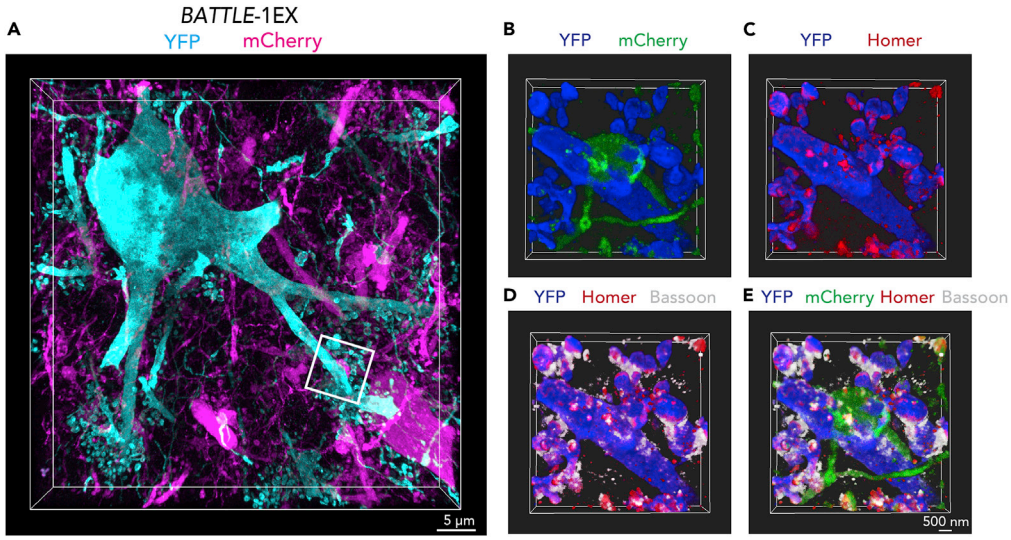

Figure 5. *BATTLE*-1EX: Three-Dimensional (3D) High-Resolution Imaging of Hilar Mossy Cells in the Hippocampus

(A) Representative maximum intensity projection 3D image of hilar mossy cells of *BATTLE*-1EX.

(B–E) Volume-rendering 3D image of box area in (A). Blue, Green, Red, and White show YFP, mCherry, Homer, and Bassoon respectively. Note that mCherry-positive presynaptic terminals form a whole synapse with YFP-positive postsynaptic spines of a mossy cell in the hippocampus.

transgene expression in transgenic animals, but it has less flexibility than a battle strategy and lacks tunability (He et al., 2017). *BATTLE*-recombinase systems have considerable potential to be applied to functional studies such as optogenetics (Fenno et al., 2011; Boyden, 2011; Kohara et al., 2014) and pharmacogenetics (Roth, 2016).

In contrast, other systems using blended multiple transgenes such as Brainbow systems (Livet et al., 2007; Weissman and Pan, 2015; Sakaguchi et al., 2018) are not suitable for these applications. The other combinatorial targeting strategies and tools are useful and versatile for functional and developmental studies of a small population of cells, like inhibitory neurons (He et al., 2016). However, they do not have either the split-tunability or sparseness-tunability of multiple transgene allocation, in contrast to *BATTLE*-recombinase systems. In addition, they are mainly based on double- or triple-transgenic mice, which are more expensive, and it takes a relatively long time to start experiments. Second, *BATTLE*-recombinase strategies produce flexible, intense, and tunable multiple sparse allocation of transgenes. Other sparse expression systems have limited expression levels (Zong et al., 2005; Tasic et al., 2012; Young et al., 2008), flexibility (Zong et al., 2005; Saunders et al., 2012; Young et al., 2008; Luo et al., 2016; Mikuni et al., 2016), and applicability; mastering the techniques is difficult (dal Maschio et al., 2012; Schubert et al., 2018). Notably, *BATTLE*-recombinase strategies have high versatility and are independent of leaky feedback expression systems based on the TetO system (Luo et al., 2016; Lin et al., 2018). Consequently, these systems have the potential to be combined with large-scale conditional TetO transgenic mice (Lewandoski, 2001).

Cre and FLP systems are widely popular, and over 1,000 Cre- and FLP-dependent AAV vectors and numerous pre-made Cre-dependent AAVs are commercially available from companies and institutions (such as Addgene). Remarkably, the *BATTLE*-recombinase system can be quickly applied and widely custom-built to standard and pre-existing Cre- and FLP-dependent AAV resources, offering a huge variety. In addition, there are also considerable floxed transgenic mouse resources for region-specific knockout studies (Lewandoski, 2001) and single-cell gene knockout studies (Kohara et al., 2007; Young et al., 2008; Luo et al., 2016; Mikuni et al., 2016). *BATTLE*-2 technology has great potential to be applied to single-cell gene knockout studies.

We combined the *BATTLE*-recombinase strategy with ExM to create *BATTLE*-1EX that enabled 3D high-resolution imaging of whole synaptic structures. Brainbow technology using multiple colors is mostly incompatible with immunohistochemistry of endogenous proteins and synaptic proteins because it uses multiple colors (Livet et al., 2007; Weissman and Pan, 2015; Sakaguchi et al., 2018). Therefore, it is insufficient to perform unambiguous identifications and dissections of whole synaptic structures and synaptic proteins. In this study, we visualized and

dissected the whole synaptic structures of local circuits in the hippocampus (DG-CA3 circuits and DG-mossy cell circuits), and *BATTLE*-1EX has the potential to be extended to other regions.

Many brain diseases are known to be accompanied by abnormal morphologies in dendrites (Irie et al., 2014) and synaptic structures (van Spronsen and Hoogenraad, 2010; Penzes et al., 2011). However, considerable efforts have been made to develop technologies for visualizing whole synaptic structures using light microscopy to understand the functions of normal mouse brains as well as the pathogenic mechanisms in the brains of disease mouse models. *BATTLE*-recombinase technologies could provide opportunities for the dissections of whole synaptic structures of the local circuits of mouse models of disease.

Recently developed and growing all-optical electrophysiology technologies (Hochbaum et al., 2014; Kannan et al., 2018; Fan et al., 2018) have great potential to reveal electrophysiological interactions between neurons in the local circuits. Because these technologies require mutually exclusive transgene expressions in many cases (Kannan et al., 2018; Fan et al., 2018), more flexible and tunable associated technologies might further facilitate the expansion of their use. Therefore, *BATTLE*-recombinase strategies might have a considerable and flexible potential to promote all-optical electrophysiology studies.

For a wide range of studies in the life sciences, both the CamKIIa promoter and other systems such as synapsin and actin promoters (Chan et al., 2017; Huda et al., 2014) could be applied to *BATTLE*-recombinase. In mouse studies, region-specific transgenic mice are well developed, but require large animal facilities and are expensive. Furthermore, the region-specific mice are insufficient to understand the homo relationship of intra-regions and intra-cell types. The *BATTLE*-recombinase systems might offer more flexible approaches to understanding the local circuits and cell interactions in the regions and cell groups.

Limitations of the Study

We acknowledge that in the current study the *BATTLE*-recombinase systems could be applied to local regions, like the hippocampus, but not global regions. Future studies may update *BATTLE*-recombinase systems to enable split-tunable allocations of multiple transgenes at the whole-body level.

Resource Availability

Lead Contact

Further information and requests for resources and reagents should be directed to and will be fulfilled by the Lead Contact, Keigo Kohara (koharake@hirakata.kmu.ac.jp).

Materials Availability

All unique/stable reagents generated in this study are available from the Lead Contact with a completed Materials Transfer Agreement.

Data and Code Availability

This study did not generate/analyze datasets and code.

METHODS

All methods can be found in the accompanying Transparent Methods supplemental file.

SUPPLEMENTAL INFORMATION

Supplemental Information can be found online at https://doi.org/10.1016/j.isci.2020.101248.

ACKNOWLEDGMENTS

We thank Y. Tatsumi, T. Unzai, E. Oiki, K. Nitta, A. Konno, A. Onishi, and N. McCullough for their assistance with the experiments. We thank H. Matsuda for her encouragement. This research was partially supported by the program for Brain Mapping by Integrated Neurotechnologies for Disease Studies (Brain/MINDS) from the Japan Agency for Medical Research and Development, AMED under the Grant Number JP19 dm0207057. This study was supported by Center for Medical Research and Education, Graduate School of Medicine, Osaka University, and grants from JSPS (16H03304, 19H03534, and 19K22583) and the Takeda Science Foundation to K.K.

AUTHOR CONTRIBUTIONS

K.K. conceived, designed, and performed the *BATTLE*-recombinase experiments. A.I., T.K., and K.K. performed the ExM experiments. H.H. packaged the lentiviruses and AAVs. K.K. and M.M. performed the viral molecular experiments. Y.N., R.B., and C.K. performed the experiments using mice. K.K, C.K., and A.I. performed quantitative analysis. K.K and A.I. wrote the manuscript. K.K. supervised the entire project.

DECLARATION OF INTERESTS

The authors declare no competing interests.

Received: September 20, 2019
Revised: October 2, 2019
Accepted: June 4, 2020
Published: June 26, 2020

REFERENCES

Ai, H.W., Henderson, J.N., Remington, S.J., and Campbell, R.E. (2006). Directed evolution of a monomeric, bright and photostable version of Clavularia cyan fluorescent protein: structural characterization and applications in fluorescence imaging. Biochem. J. *400*, 531–540.

Anastassiadis, K., Fu, J., Patsch, C., Hu, S., Weidlich, S., Duerschke, K., Buchholz, F., Edenhofer, F., and Stewart, A.F. (2009). Dre recombinase, like Cre, is a highly efficient site-specific recombinase in E. coli, mammalian cells and mice. Dis. Model Mech. *2*, 508–515.

Arenkiel, B.R., and Ehlers, M.D. (2009). Molecular genetics and imaging technologies for circuit-based neuroanatomy. Nature *461*, 900–907.

Asano, S.M., Gao, R., Wassie, A.T., Tillberg, P.W., Chen, F., and Boyden, E.S. (2018). Expansion microscopy: protocols for imaging proteins and RNA in cells and tissues. Curr. Protoc. Cell Biol. *80*, e56.

Benson, D.L., Isackson, P.J., Gall, C.M., and Jones, E.G. (1992). Contrasting patterns in the localization of glutamic acid decarboxylase and Ca2+/calmodulin protein kinase gene expression in the rat central nervous system. Neuroscience *46*, 825–849.

Boyden, E.S. (2011). A history of optogenetics: the development of tools for controlling brain circuits with light. F1000 Biol. Rep. *3*, 11.

Chan, K.Y., Jang, M.J., Yoo, B.B., Greenbaum, A., Ravi, N., Wu, W.L., Sánchez-Guardado, L., Lois, C., Mazmanian, S.K., Deverman, B.E., et al. (2017). Engineered AAVs for efficient noninvasive gene delivery to the central and peripheral nervous systems. Nat. Neurosci. *20*, 1172–1179.

Chen, F., Tillberg, P.W., and Boyden, E.S. (2015). Expansion microscopy. Science *347*, 543–548.

Chuang, K., Nguyen, E., Sergeev, Y., and Badea, T.C. (2015). Novel heterotypic rox sites for combinatorial Dre recombination strategies. G3 (Bethesda) *6*, 559–571.

dal Maschio, M., Ghezzi, D., Bony, G., Alabastri, A., Deidda, G., Brondi, M., Sato, S.S., Zaccaria, R.P., Di Fabrizio, E., Ratto, G.M., et al. (2012). High-performance and site-directed in utero electroporation by a triple-electrode probe. Nat. Commun. *3*, 960.

Dawkins, R. (1976). The Selfish Gene (Oxford University Press).

Fan, L.Z., Nehme, R., Adam, Y., Jung, E.S., Wu, H., Eggan, K., Arnold, D.B., and Cohen, A.E. (2018). All-optical synaptic electrophysiology probes mechanism of ketamine-induced disinhibition. Nat. Methods *15*, 823–831.

Fenno, L., Yizhar, O., and Deisseroth, K. (2011). The development and application of optogenetics. Annu. Rev. Neurosci. *34*, 389–412.

Gomez-Nicola, D., Riecken, K., Fehse, B., and Perry, V.H. (2014). In-vivo RGB marking and multicolour single-cell tracking in the adult brain. Sci. Rep. *4*, 7520.

Gumbiner, B.M. (1996). Cell adhesion: the molecular basis of tissue architecture and morphogenesis. Cell *84*, 345–357.

He, M., Tucciarone, J., Lee, S., Nigro, M.J., Kim, Y., Levine, J.M., Kelly, S.M., Krugikov, I., Wu, P., Chen, Y., et al. (2016). Strategies and tools for combinatorial targeting of GABAergic neurons in mouse cerebral cortex. Neuron *91*, 1228–1243.

He, L., Li, Y., Li, Y., Pu, W., Huang, X., Tian, X., Wang, Y., Zhang, H., Liu, Q., Zhang, L., et al. (2017). Enhancing the precision of genetic lineage tracing using dual recombinases. Nat. Med. *23*, 1488–1498.

Hochbaum, D.R., Zhao, Y., Farhi, S.L., Klapoetke, N., Werley, C.A., Kapoor, V., Zou, P., Kralj, J.M., Maclaurin, D., Smedemark-Margulies, N., et al. (2014). All-optical electrophysiology in mammalian neurons using engineered microbial rhodopsins. Nat. Methods *11*, 825–833.

Huda, F., Konno, A., Matsuzaki, Y., Goenawan, H., Miyake, K., Shimada, T., and Hirai, H. (2014). Distinct transduction profiles in the CNS via three injection routes of AAV9 and the application to generation of a neurodegenerative mouse model. Mol. Ther. Methods Clin. Dev. *6*, 14032.

Irie, T., Matsuzaki, Y., Sekino, Y., and Hirai, H. (2014). Kv3.3 channels harbouring a mutation of spinocerebellar ataxia type 13 alter excitability and induce cell death in cultured cerebellar Purkinje cells. J. Physiol. *592*, 229–247.

Kannan, M., Vasan, G., Huang, C., Haziza, S., Li, J.Z., Inan, H., Schnitzer, M.J., and Pieribone, V.A. (2018). Fast, in vivo voltage imaging using a red fluorescent indicator. Nat. Methods *15*, 1108–1116.

Kohara, K., Yasuda, H., Huang, Y., Adachi, N., Sohya, K., and Tsumoto, T. (2007). A local reduction in cortical GABAergic synapses after a loss of endogenous brain-derived neurotrophic factor, as revealed by single-cell gene knock-out method. J. Neurosci. *27*, 7234–7244.

Kohara, K., Pignatelli, M., Rivest, A.J., Jung, H.Y., Kitamura, T., Suh, J., Frank, D., Kajikawa, K., Mise, N., Obata, Y., et al. (2014). Cell type-specific genetic and optogenetic tools reveal hippocampal CA2 circuits. Nat. Neurosci. *17*, 269–279.

Lao, Z., Raju, G.P., Bai, C.B., and Joyner, A.L. (2012). Mosaic mutant Analysis with Spatial and Temporal control of Recombination (MASTR): a new technique for determining the fate of mutant cells using conditional floxed alleles in mice. Cell Rep. *2*, 386–396.

Lewandoski, M. (2001). Conditional control of gene expression in the mouse. Nat. Rev. Genet. *2*, 743–755.

Lin, R., Wang, R., Yuan, J., Feng, Q., Zhou, Y., Zeng, S., Ren, M., Jiang, S., Ni, H., Zhou, C., et al. (2018). Cell-type-specific and projection-specific brain-wide reconstruction of single neurons. Nat. Methods *15*, 1033–1036.

Livet, J., Weissman, T.A., Kang, H., Draft, R.W., Lu, J., Bennis, R.A., Sanes, J.R., and Lichtman, J.W. (2007). Transgenic strategies for combinatorial expression of fluorescent proteins in the nervous system. Nature *450*, 56–62.

Luo, W., Mizuno, H., Iwata, R., Nakazawa, S., Yasuda, K., Itohara, S., and Iwasato, T. (2016). Supernova: a versatile vector system for single-cell labeling and gene function studies in vivo. Sci. Rep. *6*, 35747.

Mikuni, T., Nishiyama, J., Sun, Y., Kamasawa, N., and Yasuda, R. (2016). High-throughput, high-resolution mapping of protein localization in mammalian brain by in vivo genome editing. Cell *165*, 1803–1817.

Nagy, A. (2000). Cre recombinase: the universal reagent for genome tailoring. Genesis *26*, 99–109.

Nimchinsky, E.A., Sabatini, B.L., and Svoboda, K. (2002). Structure and function of dendritic spines. Annu. Rev. Physiol. *64*, 313–353.

Penzes, P., Cahill, M.E., Jones, K.A., VanLeeuwen, J.E., and Woolfrey, K.M. (2011). Dendritic spine pathology in neuropsychiatric disorders. Nat. Neurosci. *14*, 285–293.

Pontes-Quero, S., Heredia, L., Casquero-García, V., Fernández-Chacón, M., Luo, W., Hermoso, A., Bansal, M., Garcia-Gonzalez, I., Sanchez-Muñoz, M.S., Perea, J.R., et al. (2017). Dual ifgMosaic: a versatile method for multispectral and combinatorial mosaic gene-function analysis. Cell *170*, 800–814.

Rochefort, N.L., and Konnerth, A. (2012). Dendritic spines: from structure to in vivo function. EMBO Rep. *13*, 699–708.

Roth, B.L. (2016). DREADDs for neuroscientists. Neuron *89*, 683–694.

Sakaguchi, R., Leiwe, M.N., and Imai, T. (2018). Bright multicolor labeling of neuronal circuits with fluorescent proteins and chemical tags. Elife *7*, e40350.

Saunders, A., Johnson, C.A., and Sabatini, B.L. (2012). Novel recombinant adeno-associated viruses for Cre activated and inactivated transgene expression in neurons. Front. Neural Circuits *6*, 47.

Schlake, T., and Bode, J. (1994). Use of mutated FLP recognition target (FRT) sites for the exchange of expression cassettes at defined chromosomal loci. Biochemistry *33*, 12746–12751.

Schubert, R., Trenholm, S., Balint, K., Kosche, G., Cowan, C.S., Mohr, M.A., Munz, M., Martinez-Martin, D., Fläschner, G., Newton, R., et al. (2018). Virus stamping for targeted single-cell infection in vitro and in vivo. Nat. Biotechnol. *36*, 81–88.

van Spronsen, M., and Hoogenraad, C.C. (2010). Synapse pathology in psychiatric and neurologic disease. Curr. Neurol. Neurosci. Rep. *10*, 207–214.

Südhof, T.C., and Malenka, R.C. (2008). Understanding synapses: past, present, and future. Neuron *60*, 469–476.

Tasic, B., Miyamichi, K., Hippenmeyer, S., Dani, V.S., Zeng, H., Joo, W., Zong, H., Chen-Tsai, Y., and Luo, L. (2012). Extensions of MADM (mosaic analysis with double markers) in mice. PLoS One *7*, e33332.

Tillberg, P.W., Chen, F., Piatkevich, K.D., Zhao, Y., Yu, C.C., English, B.P., Gao, L., Martorell, A., Suk, H.J., Yoshida, F., et al. (2016). Protein-retention expansion microscopy of cells and tissues labeled using standard fluorescent proteins and antibodies. Nat. Biotechnol. *34*, 987–992.

Weissman, T.A., and Pan, Y.A. (2015). Brainbow: new resources and emerging biological applications for multicolor genetic labeling and analysis. Genetics *199*, 293–306.

Young, P., Qiu, L., Wang, D., Zhao, S., Gross, J., and Feng, G. (2008). Single-neuron labeling with inducible cre-mediated knockout in transgenic mice. Nat. Neurosci. *11*, 721–728.

Zong, H., Espinosa, J.S., Su, H.H., Muzumdar, M.D., and Luo, L. (2005). Mosaic analysis with double markers in mice. Cell *121*, 479–942.

iScience, Volume *23*

Supplemental Information

BATTLE: Genetically Engineered Strategies for Split-Tunable Allocation of Multiple Transgenes in the Nervous System

Keigo Kohara, Akitoshi Inoue, Yousuke Nakano, Hirokazu Hirai, Takuya Kobayashi, Masato Maruyama, Ryosuke Baba, and Chiho Kawashima

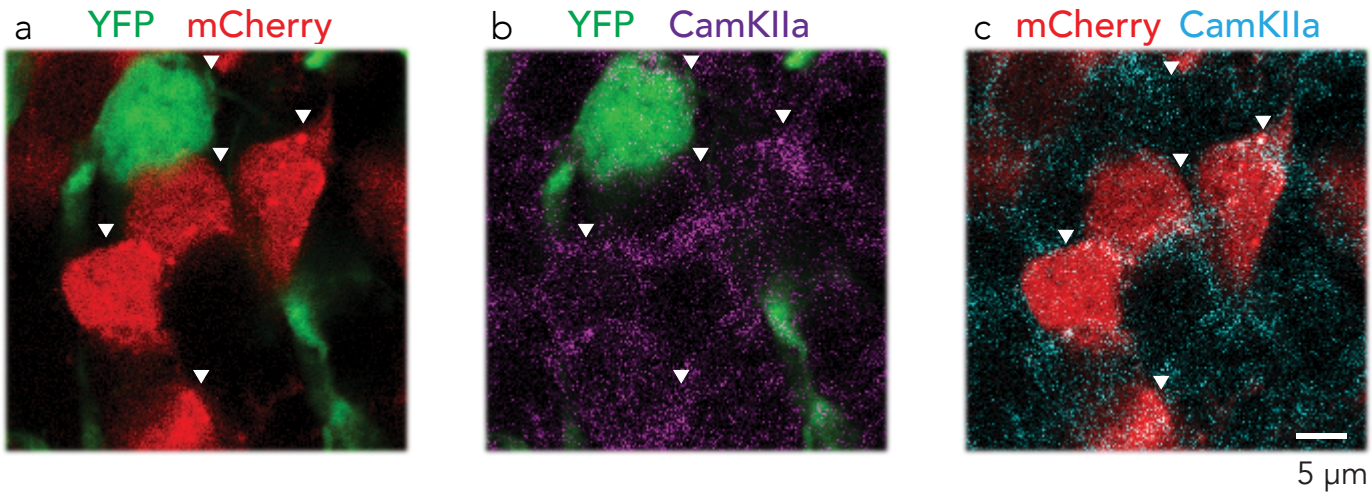

Figure S1. Specific transgene expressions of YFP and mCherry in excitatory neurons, Related to Figure 1.

a, Representative confocal image of dentate gyrus in hippocampus injected with BATTLE-1. Arrowheads indicate YFP-positive and mCherry-positive granule neurons. **b**, Specific transgene expression of YFP in CamKIIa expressing excitatory granule neurons. Magenta color shows CamKIIa immunoreactivity. **c**, Specific expression of mCherry in CamKIIa expressing excitatory granule neurons. Cyan color shows CamKIIa immunoreactivity. Scale bar represents 5 μm.

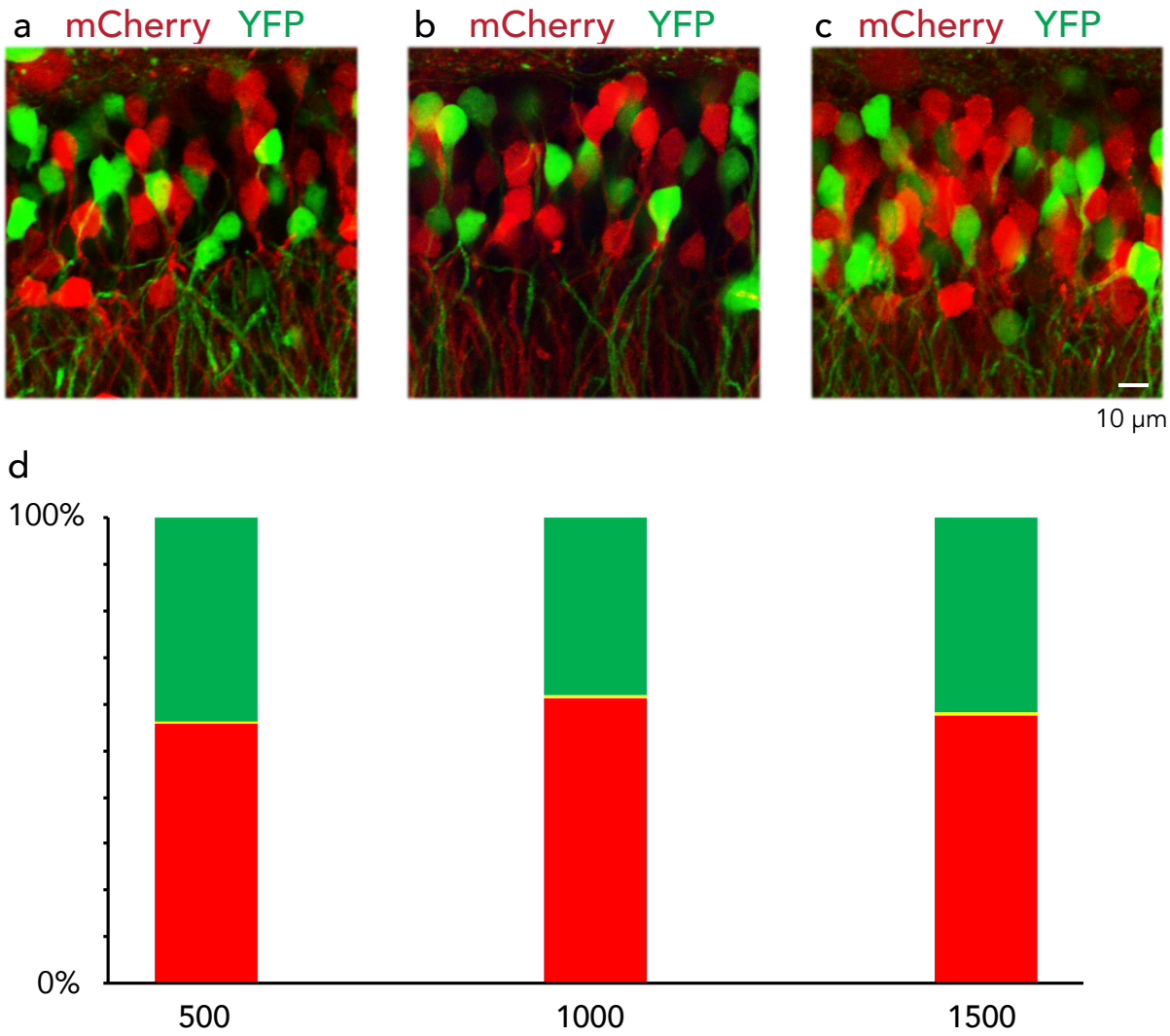

Figure S2. Splitting allocations of YFP and mCherry to granule neurons injected with BATTLE-1 at 500, 1000, and 1500 nL dosages, Related to Figure 1.

a-c, Representative maximum intensity projection image of dentate gyrus in the hippocampus injected with BATTLE-1 at 500, 1000, and 1500 nL dosages of mixed lentiviruses. Scale bar represents 10 μm. **d**, Quantification of the percentage of cells expressing fluorescent proteins in the dentate gyrus injected with BATTLE-1 (left, 500 nL; middle, 100 nL; right, 1500 nL). Red, green, and yellow represent the percentage of cells expressing mCherry-positive, YFP-positive, and YFP- and mCherry- double-positive granule neurons, respectively. For the 1000 nL dosage, the percentage of cells that were mCherry-positive, YFP-positive, and YFP- and mCherry- double positive were 61.3, 38.0, and 0.7%, respectively.

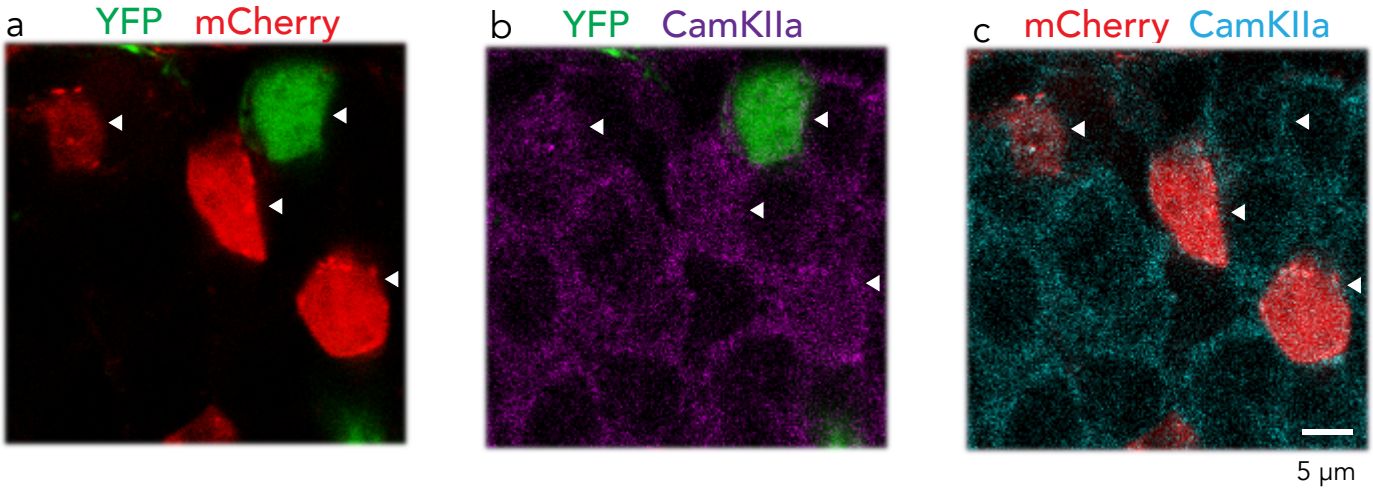

Figure S3. Specific transgene expressions of YFP and mCherry in excitatory neurons injected with *BATTLE*-2, Related to Figure 2.

a, Representative confocal image of dentate gyrus in the hippocampus injected with *BATTLE*-2. Arrowheads indicate YFP-positive and mCherry-positive granule neurons. **b**, Specific transgene expression of YFP in CamKIIa expressing excitatory granule neurons. Magenta represents CamKIIa immunoreactivity. **c**, Specific expression of mCherry in CamKIIa expressing excitatory granule neurons. Cyan represents CamKIIa immunoreactivity. Scale bar represents 5 μm.

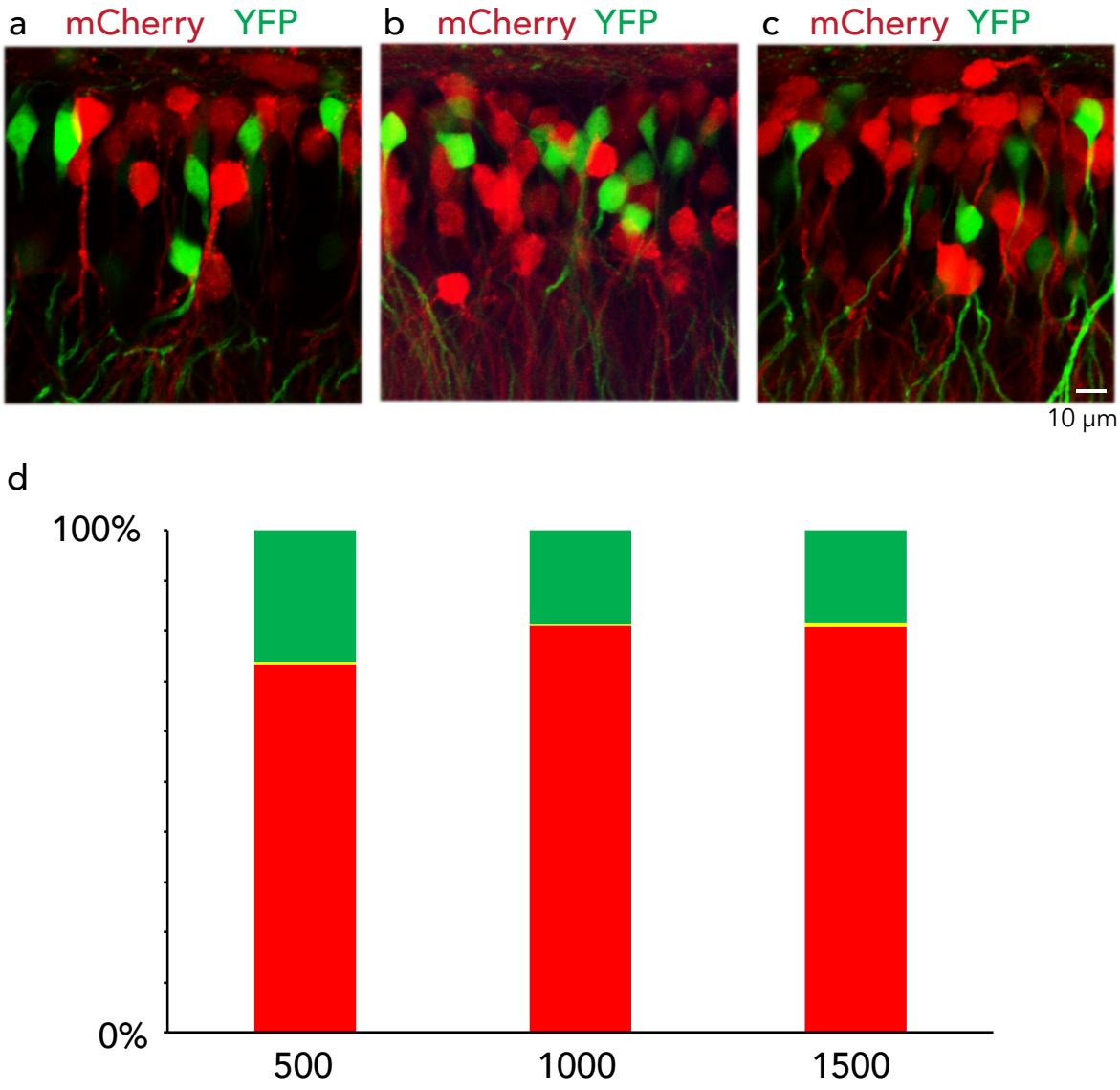

Figure S4. Splitting allocations of YFP and mCherry to granule neurons injected with *BATTLE*-2 at 500, 1000, and 1500 nL dosages, Related to Figure 2.

a-c, Representative maximum intensity projection images of dentate gyrus in the hippocampus injected with *BATTLE*-2 at 500, 1000, and 1500 nL dosages of mixed lentiviruses. Scale bar represents 10 μm. **d**, Quantification of the percentage of cells expressing fluorescent proteins in the dentate gyrus injected with *BATTLE*-2 (left, 500 nL; middle, 1000 nL; right, 1500 nL). Red, green, and yellow represent the percentage of cells expressing mCherry-positive, YFP-positive, and YFP- and mCherry- double-positive granule neurons, respectively.

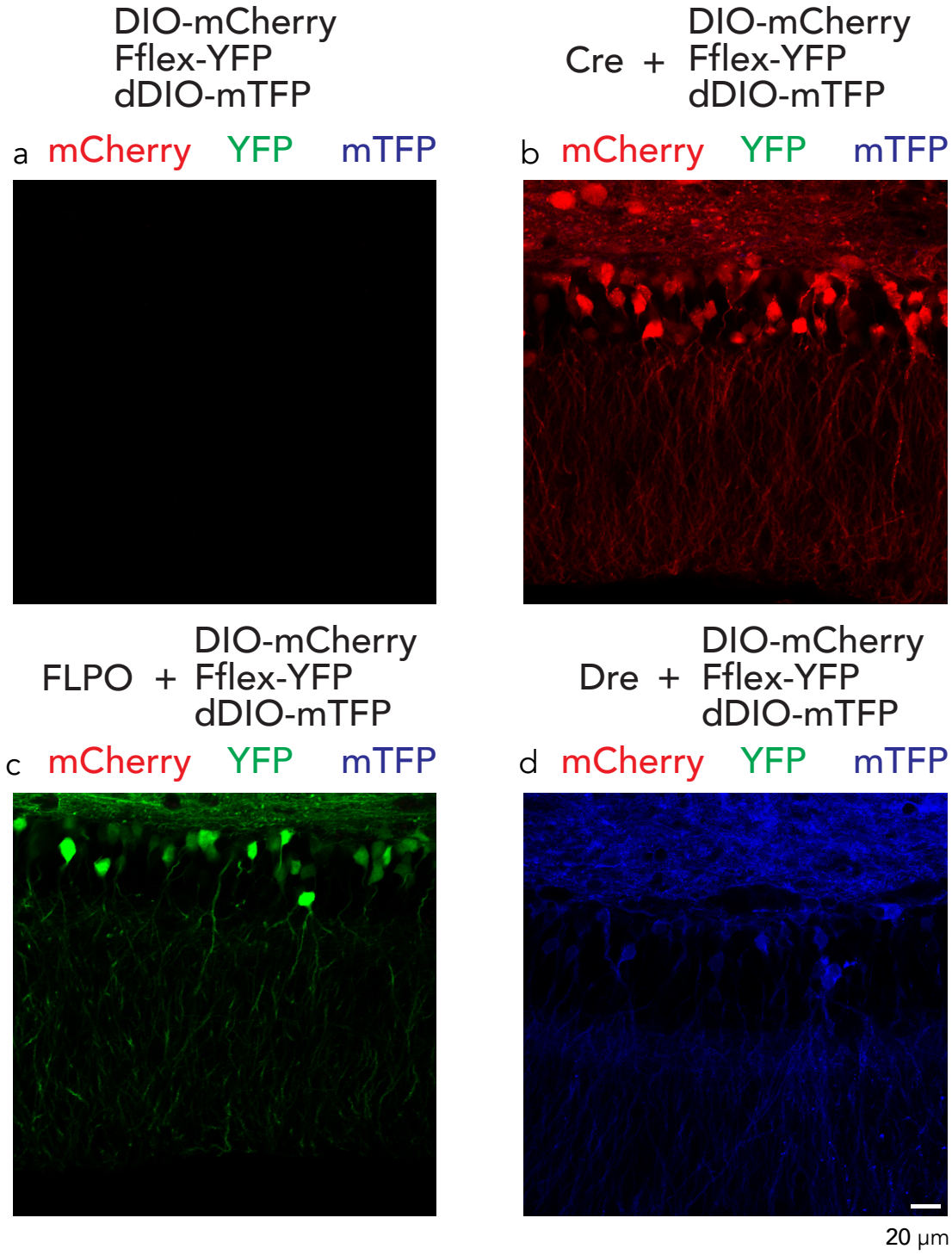

Figure S5. Recombinase-specific transgene expression of Cre-, FLPO-, and Dre-dependent AAV, Related to Figure 3.

a, Representative confocal image of dentate gyrus in hippocampus after injections of AAV-Ef1a-DIO-mCherry, AAV-EF1a-F-flex-YFP, and AAV-Ef1a-dDIO-mTFP. **b**, Representative confocal image of dentate gyrus in hippocampus after injections of lentivirus expressing Cre recombinase, AAV-Ef1a-DIO-mCherry, AAV-EF1a-F-flex-YFP, and AAV-Ef1a-dDIO-mTFP. **c**, Representative confocal image of dentate gyrus in hippocampus after injections of lentivirus expressing FLPO recombinase, AAV-Ef1a-DIO-mCherry, AAV-EF1a-F-flex-YFP, and AAV-Ef1a-dDIO-mTFP. **d**, Representative confocal image of dentate gyrus in hippocampus after injections of lentivirus expressing Dre recombinase, AAV-Ef1a-DIO-mCherry, AAV-EF1a-F-flex-YFP, and AAV-Ef1a-dDIO-mTFP. Scale bar represents 20 µm.

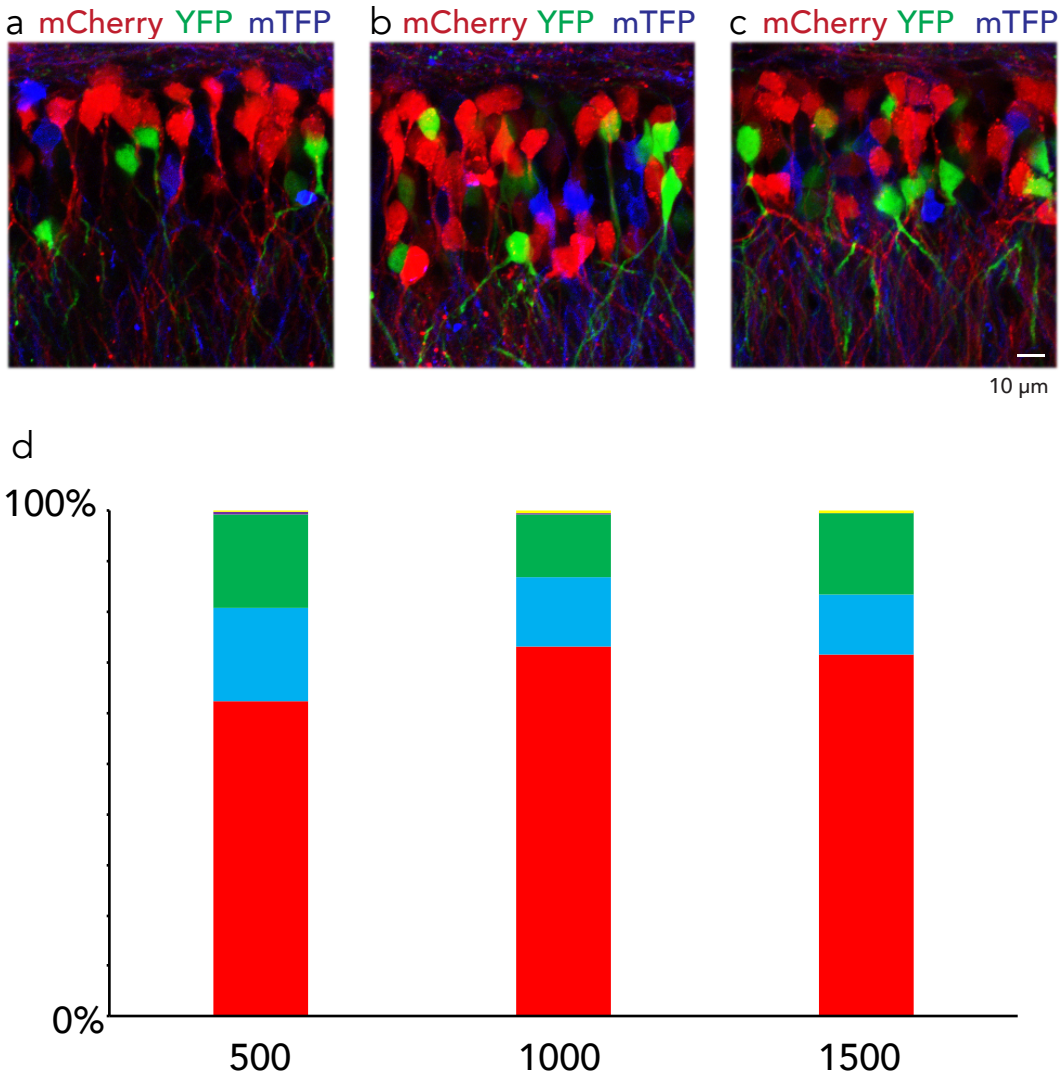

Figure S6. Triple splittable allocations of YFP, mTFP, and mCherry to granule neurons injected with *BATTLE*-2.1 at 500, 1000, and 1500 nL dosages, Related to Figure 3.
a-c, Representative maximum intensity projection images of dentate gyrus in the hippocampus injected with *BATTLE*-2.1 at 500, 1000, and 1500 nL dosages of mixed lentiviruses. Scale bar represents 10 μm. **d**, Quantification of the percentage of cells expressing fluorescent proteins in the dentate gyrus injected with *BATTLE*-2.1 (left, 500 nL; middle, 100 nL; right, 1500 nL). Red, blue, green, yellow, and purple represent the percentage of cells expressing mCherry-positive, mTFP-positive, YFP-positive, YFP- and mCherry- double-positive, and mTFP- and mCherry- double-positive granule neurons, respectively.

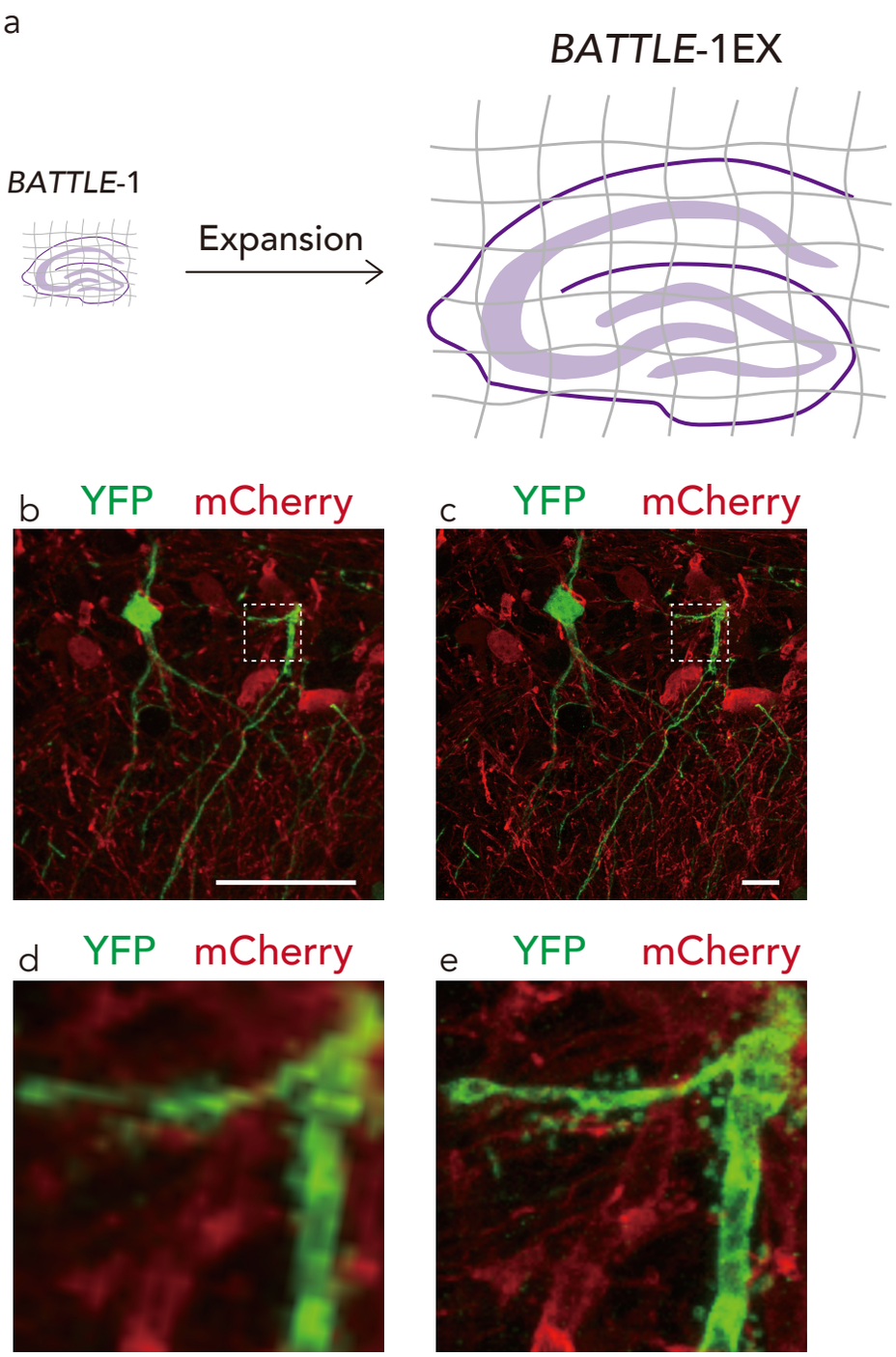

Figure S7. Comparison of sample images between pre- and post-expansion in *BATTLE*-1EX, Related to Figure 4.

a, Schematic images of pre- and post-expansion samples in *BATTLE*-1EX. **b and c**, Representative maximum intensity projection 2D images of hippocampal pyramidal neurons were compared between pre-expansion (b) and post-expansion (c). Scale bars: 50 μm. **d and e**, Magnified views of boxed regions in (b) and (c), respectively.

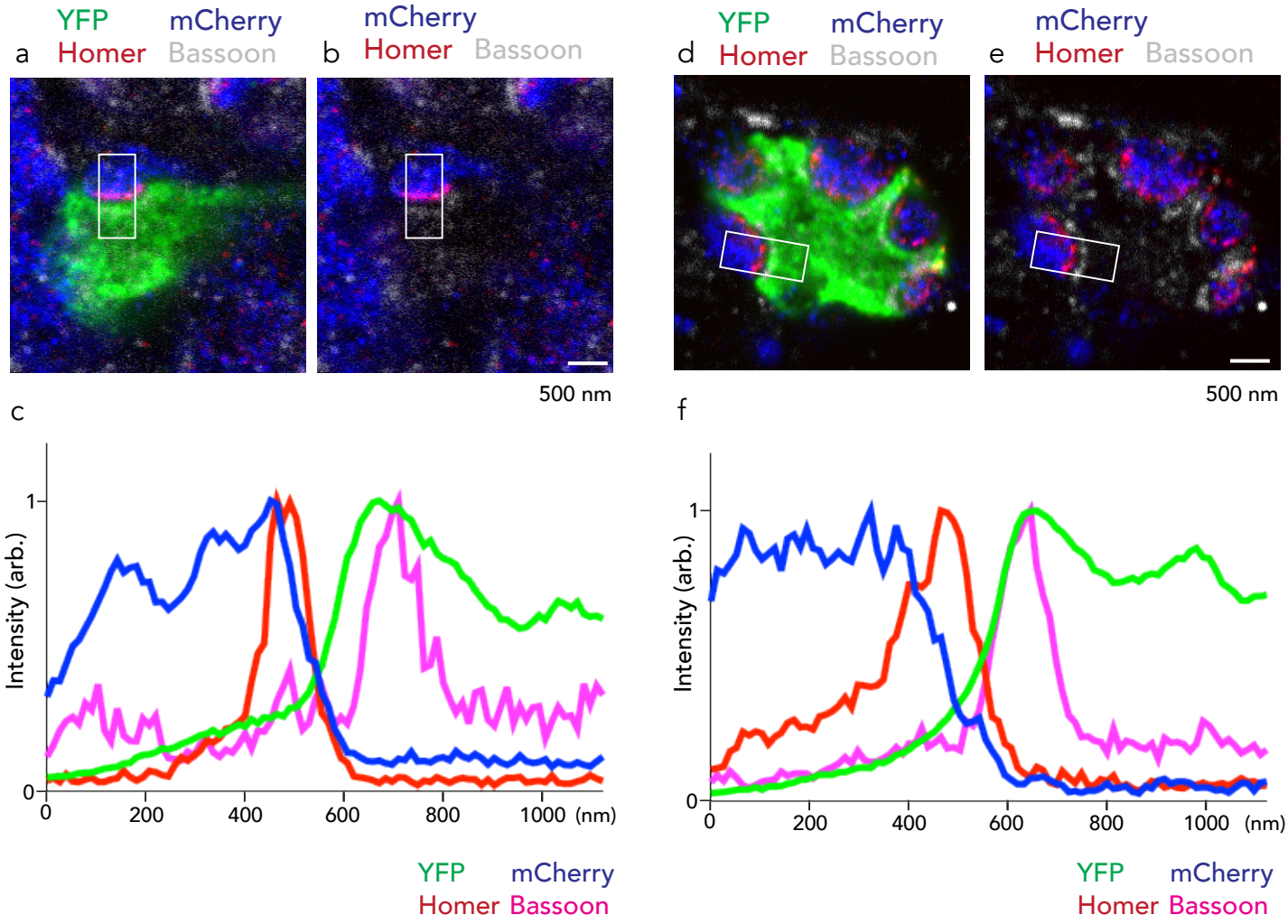

Figure S8. Other representative images of high-resolution imaging of DG-CA3 synapses in the hippocampus using *BATTLE*-1EX, Related to Figure 4.

a and **b**, Representative confocal image of DG-CA3 synapses using *BATTLE*-1EX. **c**, Line profiling analysis of boxes in a and b. **d** and **e**, Another representative confocal image of DG-CA3 synapses using *BATTLE*-1EX. **f**, Another line profiling analysis of boxes in d and e. Scale bars represent 500 nm.

Transparent Methods

Experiments were conducted in accordance with Kansai Medical University regulations and approved by the committee on Animal Care. Mice were housed as 2–5 littermates per cage with a regular dark-light cycle and access to water and food. Post-surgery mice were individually housed.

Generation of viruses

To create the lentivirus-CamKIIa (1.3 kb)-FRT5-iCre-FRT5-WPRE vector, a synthesized transgene FRT5-iCre-FRT5 was inserted into the BamHI-EcoRI site of the lentiviral backbone vector (Addgene 20943). Then, a synthesized transgene loxN-FLPO-loxN was also inserted into the BamHI-EcoRI site of the lentiviral backbone vector (Addgene 20943) to create lentivirus-CamKIIa(1.3 kb)-loxN-FLPO-loxN-WPRE vector. For *BATTLE*-2 viral Cre vectors, a synthesized transgene BamHI-FRT5-rox-AgeI was inserted into the BamHI-AgeI site of lentivirus-CamKIIa(1.3 kb)-FRT5-iCre-FRT5-WPRE vector.

Then, a synthesized transgene NheI-rox-FRT5-EcoRI was inserted into the Nhe-EcoRI site of lentivirus-CamKIIa(1.3 kb)-FRT5-rox-iCre-FRT5-WPRE vector. For *BATTLE*-2 viral FLPO vectors, synthesized transgene BamHI-loxN-rox-AgeI was

inserted into the BamHI-AgeI site of lentivirus-CamKIIa (1.3 kb)-loxN-FLPO-loxN-WPRE vector. A synthesized transgene NheI-rox-loxN-EcoRI was inserted into the NheI-EcoRI site of lentivirus-CamKIIa (1.3 kb)-loxN-rox-FLPO-loxN-WPRE vector to create the lentivirus-CamKIIa(1.3 kb)-loxN-rox-FLPO-rox-loxN-WPRE vector.

For *BATTLE*-2 viral shadow Dre vectors, a synthesized transgene BamHI-FRT5-loxN-Dre-LoxN-FRT5-EcoRI was inserted into the BamHI-EcoRI site of the lentivirus-CamKIIa (1.3 kb) backbone vector to create the lentivirus-CamKIIa (1.3 kb)-FRT5-loxN-Dre-LoxN-FRT5-WPRE vector. These five lentiviruses were packaged at Gunma University. For AAV vectors, a synthesized transgene NheI-YFP-BSrGI was inserted into the NheI-BSrGI site of AAV F-Flex backbone vector (Addgene 60661) to create the AAV-EF1a-F-flex-YFP vector. A synthesized transgene KpNI-Rox12-Rox2-speI-reverse complement mTFP-reverse complement Rox12-reverse complement Rox2-EcoRI was inserted into the KpnI-EcoRI site of pAAV-EF1a-double floxed-hChR2(H134R)-EYFP-WPRE-HGHpA vector (Addgene 20298) to create AAV-Ef1a-dDIO-mTFP. AAV-Ef1a-DIO-mCherry (Addgene Plasmid 47636), AAV-EF1a-F-flex-YFP, and AAV-Ef1a-dDIO-mTFP were packaged at Gunma University.

Stereotaxic injections of viruses

Mice were anesthetized with isoflurane and placed in a stereotaxic apparatus (World Precision Instruments). Tapered glass capillaries were processed by Micropipette Puller (Sutter). The tapered glass capillary and Hamilton syringe with a 26-gauge needle were filled with mineral oil and used to inject the viruses that were injected into the hippocampal DG-CA2-3 area in the right hemisphere at the predetermined coordinates (-1.94 mm AP, +2.14 mm ML, -2.32 mm DV) from the bregma. For *BATTLE*-1 viruses, adult mice were infected with 1 μL mixed lentiviruses (lenti-CamKIIa-FRT5-Cre-FRT5:lenti-CamKIIa-loxN-FLPO-loxN=1:1 [each virus consisted of 5×10E8 copies] or lenti-Cre:lenti-FLPO=1:0.01 [5×10E8 and 5×10E6 copies, respectively]) with the first injections. For *BATTLE*-1 virus dosage experiments, adult mice were infected with 500 nL or 1500 nL mixed lentiviruses (lenti-CamKIIa-FRT5-Cre-FRT5:lenti-CamKIIa-loxN-FLPO-loxN=1:1).

Three weeks later, AAV-EF1a-DIO-mCherry (1 μL, titer: 1.43×10E13) and AAV-EF1a-DIO-YFP (1 μL, titer: 1.43×10E13) were mixed and injected at the same sites used for the first injections. The mice were then perfused 1 week after the second injections. For *BATTLE*-2 virus injections for splitting transgene expression, adult mice were infected with *BATTLE*-2 lentiviruses (1 μL, Lenti-CamKIIa-FRT5-rox-Cre-FRT5:lenti-CamKIIa-loxN-rox-FLPO-rox-loxN:lenti-CamKIIa FRT5-loxN-Dre-loxN-

FRT5=1:1:1, each virus consisted of 3×10E8 copies) with the first injections. For *BATTLE*-2 virus dosage experiments, adult mice were infected with 500 nL or 1500 nL mixed lentiviruses (Lenti-CamKIIa-FRT5-rox-Cre-FRT5:lenti-CamKIIa-loxN-rox-FLPO-rox-loxN:lenti-CamKIIa-FRT5-loxN-Dre-loxN-FRT5=1:1:1). Three weeks later, AAV-EF1a-DIO-mCherry and AAV-EF1a-DIO-YFP (both 1 μL, titer: 1.43×10E13) were mixed and injected at the same sites used for the first injections. The mice were perfused 1 week after the second injections. For *BATTLE-2.1* triple-color virus experiments, adult mice were infected with 500 nL or 1000 nL or 1500 nL mixed lentiviruses (Lenti-CamKIIa-FRT5-rox-Cre-FRT5:lenti-CamKIIa-loxN-rox-FLPO-rox-loxN:lenti-CamKIIa FRT5-loxN-Dre-loxN-FRT5=1:1:1). Three weeks later, AAV-EF1a-DIO-mCherry, AAV-EF1a-fFlex-YFP, and AAV-Ef1a-dDIO-mTFP (all 667 nL, titer: 1.81×10E13) were mixed and injected at the same sites used for the first injections. For crosstalk control experiments, AAV-EF1a-DIO-mCherry, AAV-EF1a-fFlex-YFP, and AAV-Ef1a-dDIO-mTFP (all 667 nL, titer: 1.81×10E13) were mixed and injected into the hippocampus. The mice were then perfused 1 week after the second injections.

For crosstalk recombinase experiments, adult mice were infected with 1 μL lenti-CamKIIa-FRT5-loxN-Dre-loxN-FRT5 or lenti-CamKIIa-FRT5-rox-Cre-rox-FRT5 or lenti-CamKIIa-loxN-rox-FLPO-rox-loxN (viruses consisted of 0.5×10E9 copies). Then,

AAV-EF1a-DIO-mCherry, AAV-EF1a-fFlex-YFP, and AAV-Ef1a-dDIO-mTFP (all 667 nL, titer: 1.81×10E13) were injected on the same day as the first injections. The mice were then perfused 1 week after the second injections.

For *BATTLE*-2 virus injections of multi-sparse transgene expressions, adult mice were infected with 1 μL lenti-CamKIIa-FRT5-loxN-Dre-loxN-FRT5:lenti-CamKIIa-FRT5-rox-Cre-FRT5:lenti-CamKIIa-loxN-rox-FLPO-rox-loxN=200:1:10 (viruses consisted of 1×10E9, 5×10E6, and 5×10E7 copies, respectively). Then, AAV-EF1a-DIO-mCherry and AAV-EF1a-DIO-YFP (1 μL, titer: 1.43×10E13) were injected on the same day as the first injections. The mice were perfused 2 weeks after the viral injections. Adult mice were infected with conventional AAV-CAG-GFP viruses (Addgene 37825-AAVrg, 1 μL, titer 1×10E13) and then they were perfused 7 days later.

Immunohistochemistry

Adult mice were anesthetized with a mixture of medetomidine, midazolam, and butorphanol, and then transcardially perfused with ice-cold 4% (w/v) paraformaldehyde (PFA) in phosphate-buffered saline (PBS) using a peristaltic pump. Then, the brains were post-fixed in the same solution for 24 h, transferred to 30% (w/) sucrose in PBS, and embedded in optimal cutting temperature compound (Sakura). The brains were then

frozen with isopentane and liquid nitrogen and sectioned using a cryostat (Leica, 60 μm-thick sagittal sections).

For CamKIIa staining, freely floating sections were incubated with 3% (v/v) goat serum in 0.3% Triton X-PBS for 1 h, followed by incubation with primary mouse monoclonal antibody against CamKIIa (1:300, Abcam ab22609) in 3% goat serum plus 0.3% Triton X-PBS overnight at 4 °C. After rinsing the sections three times with 0.3% Triton X-PBS for 15 min, they were incubated with secondary anti-mouse goat antibody conjugated with Alexa Fluor 647 Plus (1:1000, A32728, Thermo Fisher Scientific) for 2 h.

Then, the sections were rinsed three times with 0.3% Triton X-PBS for 15 min. Co-expression of CamKIIa and fluorescent proteins was determined based on their expressions in the cytoplasm of cell bodies in confocal images captured using an Olympus confocal microscope (FV3000). All sections were mounted on glass slides using Vector shield and visualized using 4',6-diamidino-2-phenylindole (DAPI, Vector Lab).

Fluorescence imaging

Fluorescence images were acquired using an inverted confocal fluorescent microscope (Zeiss, LSM700, LSM710 and Olympus FV3000) using 10×, 20×, 40×, 60×,

and 63× objectives. Maximum intensity projection images were generated using Zenblack software (Zeiss), FV31S-SW software (Olympus), and Imaris 9.1 (Bitplane). 3D volume rendering (Figs. 3e, f, and 4) was generated after background subtraction using Imaris 9.1 (Bitplane).

Analysis of splitting expression of fluorescent protein

To analyze the splitting allocation of YFP and mCherry, fluorescent images were captured using confocal microscopy (Zeiss LSM700) with a 20× objective lens. To analyze the splitting allocation of mTFP, YFP, and mCherry in triple-color *BATTLE*-2.1 experiments or crosstalk experiments, fluorescent images were captured using confocal microscopy (Zeiss LSM710) with a 20× objective lens, 458 nm laser, 514 nm laser, and 561 nm laser. Fluorescence intensity was measured from square regions (3.9 μm × 3.9 μm) on the cell bodies of DG granule and CA2-3 neurons in the confocal images (400 μm × 400 μm × 2 μm) using the ZenBlue 2012 software (Zeiss). The co-expressions of mTFP, YFP, and mCherry were determined when both fluorescence intensities were higher than the background fluorescence (Arbitrary unit 10).

BATTLE-*1EX (expansion microscopy of* BATTLE-*1)*

ExM (expansion microscopy) was performed according a published method with minor modifications (Asano et al., 2018). Free-floating sections were subjected to antigen retrieval in citrate buffer (10 mM citric acid plus 0.05% Tween 20, pH 8.0) at 80 °C for 30 min, and washed four times with PBS for 5 min. Sections were permeabilized and blocked with blocking buffer containing 1% bovine serum albumin (BSA), 0.1% Triton X-100 in PBS for 1 h at 26 °C. Sections were then incubated with primary chicken polyclonal antibody to GFP (1:500, ab13970, Abcam), rat monoclonal antibody to RFP (1:100, 5f8-100, Chromotek), mouse monoclonal antibody to Bassoon (1:100, ab82958, Abcam), and rabbit polyclonal antibody to Homer1 (1:100, 160003, SYSY) in blocking buffer for 2 days at 4 °C, followed by washing four times with blocking buffer for 5 min.

Sections were incubated with secondary anti-chicken donkey antibody conjugated with Alexa488 dye (1:200, 703-545-155, Jackson), anti-rat donkey antibody conjugated with Alexa568 dye (1:100, ab175710, Abcam), anti-mouse goat antibody conjugated with Atto647N dye (1:100, 50185, Rockland), and anti-rabbit goat antibody conjugated with CF405M dye 1:100, 20373, Biotium) in blocking buffer for 1 day at 4 °C, washed sequentially three times each with blocking buffer, high-salt PBS (PBS+350 mM NaCl), and PBS for 5 min each time. Anchoring treatment was performed in Acryloyl-X

(0.1 mg/mL) in PBS for more than 6 h at room temperature, washed five times with PBS for 5 min each time.

For gelation, sections were immersed in the gelling solution (monomer solution [8.6% sodium acrylate, 2.5% acrylamide, 0.15% N,N′-methylenebisacrylamide, and 11.7% NaCl in PBS] mixed with ammonium persulfate, tetramethylethylenediamine, and 4-hydroxy-TEMPO at a ratio of 47:1:1:1) for 30 min on ice. Sections were then transferred to the gelling chamber (samples were sandwiched by a glass slide and cover slip on either side of the samples for spacers), and gelled for 2 h at 37 °C.

The hippocampal regions were trimmed from gelled sections and incubated with digestion buffer (50 mM Tris-HCl [pH 8.0], 23 mM ethylenediaminetetraacetic acid [EDTA], 0.5% Triton X-100, 0.8 M guanidine HCl, and 8 U/mL ProK) overnight, washed three times with PBS for 5 min, and then stored at 4 °C in the dark until expansion. For expansion, samples were washed five times with water for 10 min before transferring to the imaging chamber where they were sandwiched between a coverslip and silicon sheets, with silicon sheets on either side as spacers. The magnification was calculated using physical distances of two landmark positions in the pre- and post-expansion images measured by Imaris 9.1 (Bitplane).

Line profiling analysis of fluorescent intensities in whole synapses

To quantify whole synaptic structures and the distributions of Homer and Bassoon, measurements were conducted on a boxed area (478 nm × 1094 nm) of the whole synaptic area. The line profiling analysis of fluorescent intensities of YFP, mCherry, Homer, and Bassoon was performed using the Image J program (National Institutes for Health [NIH]).

Reproducibility

All experiments were conducted more than three times.